Miner Deposita
DOI 10.1007/s00126-007-0144-4

ARTICLE

Hypogene Zn carbonate ores in the Angouran deposit, NW Iran

Maria Boni · H. Albert Gilg · Giuseppina Balassone · Jens Schneider · Cameron R. Allen · Farid Moore

Received: 12 March 2007 / Accepted: 22 May 2007

Abstract The world-class Angouran nonsulfide Zn–Pb deposit is one of the major Zn producers in Iran, with resources estimated at about 18 Mt at 28% Zn, mainly in the form of the Zn carbonate smithsonite. This study aims to characterize these carbonate ores by means of their mineralogy and geochemistry, which has also been extended to the host rocks of mineralization and other local carbonate rock types, including the prominent travertines in the Angouran district, as well as to the local spring waters. Petrographical, chemical, and stable isotope (O, H, C, Sr) data indicate that the genesis of the Zn carbonate ores at Angouran is fairly distinct from that of other "classical" nonsulfide Zn deposits that formed entirely by supergene processes. Mineralization occurred during two successive stages, with the zinc being derived from a preexisting sulfide ore body. A first, main stage of Zn carbonates (stage I carbonate ore) is associated with both preexisting and subordinate newly formed sulfides, whereas a second stage is characterized by supergene carbonates (Zn and minor Pb) coexisting with oxides and hydroxides (stage II carbonate ore). The coprecipitation of smithsonite with galena, pyrite and arsenopyrite, as well as the absence of Fe- and Mn-oxides/hydroxides and of any discernible oxidation or dissolution of the sphalerite-rich primary sulfide ore, shows that the fluids responsible for the main, stage I carbonate ores were relatively reduced and close to neutral to slightly basic pH with high fCO_2. Smithsonite $\delta^{18}O_{VSMOW}$ values from stage I carbonate ore range from 18.3 to 23.6‰, while those of stage II carbonate ore show a much smaller range between 24.3 and 24.9‰. The $\delta^{13}C$ values are fairly constant in smithsonite of stage I carbonate ore (3.2–6.0‰) but show a considerable spread towards lower $\delta^{13}C_{VPDB}$ values (4.6 to −11.2‰) in stage II carbonate ore. This suggests a hypogene formation of stage I carbonate ore at Angouran from low-temperature hydrothermal fluids, probably mobilized during the waning stages of Tertiary–Quaternary volcanic activity in an environment characterized by abundant travertine systems throughout the whole region. Conversely, stage II carbonate ore is unambiguously related to supergene weathering, as evidenced by the absence of sulfides, the presence of Fe-Mn-oxides and arsenates, and by high $\delta^{18}O$ values found in

Editorial handling: B. Lehmann

M. Boni (✉) · G. Balassone
Dipartimento Scienze della Terra,
Università di Napoli "Federico II",
Via Mezzocannone, 8,
80134 Naples, Italy
e-mail: boni@unina.it

M. Boni
Geologisch-Paläontologisches Institut, Universität Heidelberg,
Heidelberg, Germany

H. A. Gilg
Lehrstuhl für Ingenieurgeologie,
Technische Universität München,
Munich, Germany

J. Schneider
Département de Minéralogie, Université de Genève,
Geneva, Switzerland

C. R. Allen
Teck Cominco American,
Spokane, WA, USA

F. Moore
Geological Department, University Shiraz,
Shiraz, Iran

Present address:
J. Schneider
Geodynamics and Geofluids Research Group and Centre
for Archaeological Sciences (CAS), K.U,
Leuven, Belgium

smithsonite II. The variable, but still relatively heavy carbon isotope values of supergene smithsonite II, suggests only a very minor contribution by organic soil carbon, as is generally the case in supergene nonsulfide deposits.

Keywords Angouran · Iran · Nonsulfide zinc · Smithsonite · Stable isotopes

Introduction

Nonsulfide Zn deposits have experienced a significant revival over the recent years, as a consequence of new developments in hydrometallurgical acid-leaching, solvent-extraction, and electrowinning techniques (Boni 2003; Hitzman et al. 2003). Iran is a country particularly endowed with nonsulfide ores. Typical examples currently under exploration are, among others, the Iran-Kuh, Kuh-e-Surmeh, and Mehdi-Abad deposits, all located in the Kerman province (Ghazban et al. 1994; Borg 2005) and the smaller nonsulfide bodies of the Kuhbanan-Bahabad area (Amiri et al. 2005; Amiri and Rasa 2006). All these deposits are of Mississippi Valley-type affiliation with hypogene sphalerite + galena ores at depth, capped by irregular supergene ores closer to (paleo)surface.

The world-class, high-grade Angouran nonsulfide Zn–Pb deposit, situated in the western Takab–Zanjan province about 450 km northwest of Tehran (Fig. 1a), is one of the major Zn producers in Iran, a country whose total Zn production will attain 200,000 tonnes in 2007. Nonsulfide ore resources at Angouran are estimated at about 18 Mt of ore at 28% Zn, mainly in the form of Zn carbonates, and 4.5% Pb (Annels et al. 2003; Borg and Daliran 2004). The deposit is currently owned by Iranian Mines & Mining Industries Development & Renovation Organization (IMIDRO) and has been exploited by Iran Zinc Mines Development Company (IZMDC) in an open pit at >3,000-m elevation. Additional yet unexploited sulfide reserves amount to about 5 Mt at 40% Zn (Gilg et al. 2006). There is also a project to process a substantial volume of smithsonite-bearing tailings from earlier mining operations so as to reduce the problem of environmental pollution (Moradi et al. 2004).

The renewed interest in nonsulfide mineralization throughout the world has stimulated a new wave of scientific research on the Angouran deposit, focused both on the sulfide and nonsulfide ores (Annels et al. 2003; Daliran and Borg 2003, 2005a, b; Gilg et al. 2003a, Gilg and Boni 2004a, b; 2006; Borg and Daliran 2004). The Angouran nonsulfide ores are distinct from those known from the "classical" supergene Zn deposits elsewhere (Large 2001; Hitzman et al. 2003). One of the most striking macroscopic characteristics is the association of nonsulfides and primary sulfides, dominated by sphalerite, which are in textural equilibrium and commonly do not show any obvious indication of oxidation or dissolution. There is also a marked difference in the main and trace element contents between sulfide and nonsulfide ores (Table 1). Both factors are obviously related to the specific nature and circulation mechanisms of the mineralizing fluids that precipitated the nonsulfide assemblages as well as to the source of the metals. In earlier studies, the smithsonite-dominated nonsulfides, which represent the economically most significant part of the Angouran deposit, have been generally interpreted to be a product of exclusively supergene processes (Borg and Daliran 2004; Daliran and Borg 2003; Hitzman et al. 2003). The discovery of a unique sulfide–carbonate association in the deposit, as well as preliminary stable isotope data of the zinc carbonates (Gilg et al. 2003a), has challenged this conventional genetic interpretation. The latter authors suggested that the main stage nonsulfide ores at Angouran are of hypogene origin and precipitated from low-temperature hydrothermal fluids. This process was followed by a limited supergene mineralization phase. On the other hand, Angouran does not show the typical mineralogical characteristics of other nonsulfide deposits that have been interpreted to be of hypogene–hydrothermal origin (Hitzman et al. 2003). The main nonsulfide mineral is the Zn carbonate smithsonite, whereas willemite and hydrothermal dolomite are completely lacking. The geological setting is also totally different from other Zn silicate-dominated hypogene nonsulfide deposits like Vazante (Brazil) or Beltana (Australia), which consist of structurally controlled veins or pipe-like bodies with variably developed halos of hydrothermal dolomite.

This study, which follows a previously published paper on the Angouran sulfides (Gilg et al. 2006), focuses on the nature and origin of the Zn carbonates at Angouran. We present new mineralogical, petrographical, and (isotope) geochemical data on these ores and derive formational conditions. To trace the source of the metals and the origin of the mineralizing fluids, we have extended our analyses not only to the host rocks of the main deposit but also to several carbonate types and spring waters in the immediate surroundings of the mine and the adjacent Takab district.

Geological setting and sulfide ores

The Angouran Zn(–Pb–Ag) deposit is situated in the western Zanjan Province, NW Iran. This area belongs to the northwestern part of the Sanandaj-Sirjan Zone, a metamorphic belt within the Zagros orogen (Fig. 1a). The Zagros orogen formed by Cretaceous subduction of the Neotethys ocean, followed by Tertiary continental collision

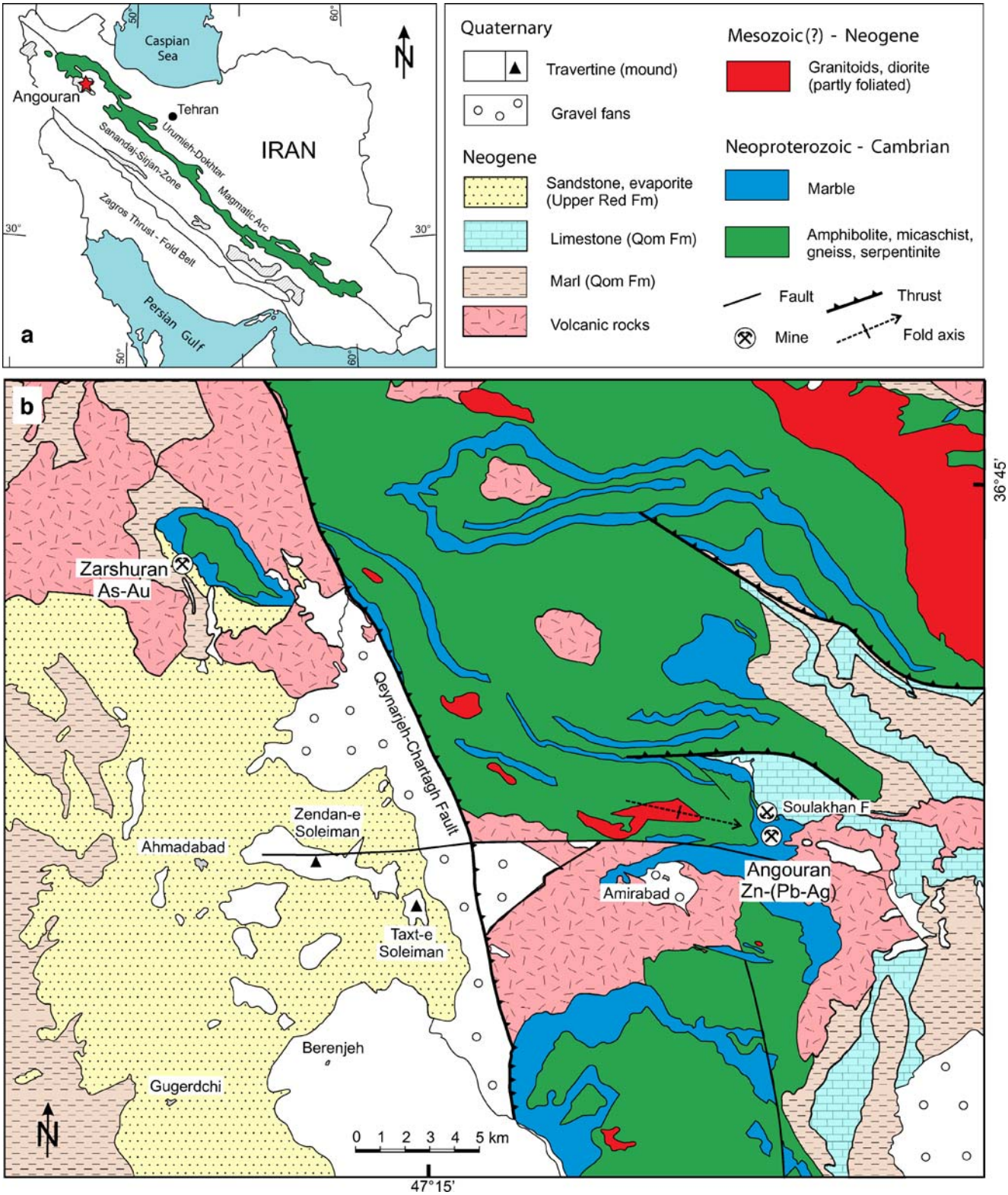

Fig. 1 **a** Location of the Angouran deposit in the Zagros orogenic belt. **b** Schematic regional geological map of the Takab–Zanjan area, with the location of the mine area, and of the sampled travertines and hot/cold spring area (after Gilg et al. 2006)

Table 1 Selected trace elements in sulfide vs carbonate ore

Element	Sulfide ore	Carbonate ore
Zn	37.70%	26.60%
Pb	1.00%	5.20%
As	760 ppm	6,100 ppm
Sb	300 ppm	570 ppm
Hg	20 ppm	10 ppm
Ag	213 ppm	35 ppm
Co	403 ppm	490 ppm
Ni	344 ppm	350 ppm
Cu	250 ppm	400 ppm

between the Afro-Arabian plate and Gondwana-derived microplates (Alavi 1994; Glennie 2000).

The Angouran deposit is hosted by a metamorphic core complex that has been rapidly exhumed during an extensional phase in the Lower Miocene (Gilg et al. 2006). This metamorphic complex (Gazanfari 1991) consists of amphibolites, serpentinites, gneisses, micaschists, and various, mainly calcitic and rarely dolomitic marbles. The marbles are in part intercalated as thin layers between schists, gneisses and amphibolites and form the more than 300-m thick, uppermost "Angouran" marble horizon that hosts the main orebody. The age of the protoliths of the metamorphic rocks are not well constrained but are presumably of Neoproterozoic (to Cambrian?) age (Hamdi 1995; Stockli et al. 2004). The metamorphic complex at Angouran shows complex internal thrusting, isoclinal folding, and a superimposed prominent open folding. Shortly after exhumation, a sequence of Miocene subvolcanic and volcanic rocks (mostly andesitic to rhyolitic pyroclastics), minor late basaltic dikes, as well as sedimentary rocks of both shallow marine (Qom Formation) and red-bed type continental origin including evaporites (Upper Red Formation), were deposited unconformably on the core complex. In the Pliocene, the metamorphic complex with its cover was thrust onto the Tertiary volcanic and sedimentary rock sequence (Stockli et al. 2004; Gilg et al. 2006), and significant uplift started. Probably during this change from a Miocene extensional to a Pliocene compressional tectonic regime, marine evaporative brines infiltrated the metamorphic complex depositing the Angouran sulfide orebody at the contact between footwall micaschists and the Angouran marbles. The sulfide orebody is tabular, replacive, associated to abundant breccias, lacks an obvious wallrock alteration, and is clearly postmetamorphic. The ore composition is simple with predominantly Fe-poor sphalerite, minor pyrite and galena, traces of Ni–Co arsenides. The main gangue comprises sulfates (mainly anhydrite, possibly barite) and minor quartz, muscovite and dolomite. In a successive stage, the sulfates have been almost completely dissolved and the cavities filled with euhedral Zn carbonates. The ore-forming fluids were Ca–Na–Cl brines of seawater evaporation origin with high and constant salinity (~24 wt.% total dissolved solids). The temperatures of ore formation are estimated from about 80 to less than 200°C at depths of less than 1–2 km (Gilg et al. 2006).

Subsequent Quaternary sediments in the Angouran area comprise widespread gravel fans, alluvium, and very extensive travertine deposits that are related to numerous low to moderately hot springs in the area. Most travertines are located to the west of the Qeynarjeh-Chartagh fault, on the gypsiferous Upper Red Formation of the Takab depression (2,100–2,200 m a.s.l.) and follow 55° (NE-SW), 90° (E-W), and 120° (NW-SE) striking structures (Damm 1968). Examples are the large Berenjeh travertine field with a length of 3 km, a width of 1.7 km, a thickness of at least 200 m (Damm 1968), and the E-W-trending, 4 km long and 1.3 km wide Zendan travertine field with many still active hot springs (11–39°C) near Ahmadabad as well as the remarkable 110-m-high Zendan-e Soleiman travertine mound (Figs. 1b and 2b). This volcano-like cone contains a hollow cylindrical feeder channel with 70-m diameter (Zendan-e Soleiman means Solomon's prison) and was probably filled with hot water about 2,500–3,000 years ago, as suggested by archeological remains on the flanks of the cone (Naumann 1961). Damm (1968) estimated that the cone took about 10,000 years to form from an artesian spring. The nearby Taxt-e Soleiman (Solomon's throne) travertine mound with a height of 50 m still contains a circular spring lake with a diameter of 110 m and 64-m depth (Geological Survey of Iran 1999). The 18–21°C warm spring at Taxt-e Soleiman is the most productive in the area with about 100 l/s (Damm 1968; Naumann 1961). The mound is host to a Zoroastrian fire temple and to Sassanian remains. Other smaller travertine deposits and hot spring areas are located near the Zarshuran (As-Au) and Agh-Darreh (Sb-Au) mines (Damm 1968). The hot springs in the Takab geothermal field are of mostly artesian origin, with temperatures ranging from 11 to 50°C (Houtum-Schindler 1881; Damm 1968). They discharge strongly mineralized (0.7–2.0 g TDS/l) Ca-HCO_3 waters with elevated sulfate contents (up to 0.69 g/l), often accompanied by degassing, and have a pH of 6.4–7.8 (Damm 1968). The spring gases are CO_2-rich (96 vol.%) and contain minor H_2S (0.4 vol.%), N_2 (2 vol.%), and O_2 + Ar (0.4 vol.%). The muddy sediments in the Taxt-e Soleiman warm spring contain about 4 wt.% Fe, 1.62 wt.% As, and traces of Zn (Naumann 1961). Earthquakes are frequent in the region and influence the discharge and temperature of the hot springs (Houtum-Schindler 1881). The commonly encountered cold springs in the Angouran region have temperatures of less than 10°C, mostly around 8°C (Houtum-Schindler 1881).

The only significant travertine deposits in the mountainous area to the east of the Qeynarjeh-Chartagh fault is located

along the E-W trending Zendan-e Soleiman fault only 500 m to the east of the Angouran mine. Over an area of 3-km length and up to 0.5-km width, a series of cascade-like travertine plateaus stretch from the discharge area at a minimum elevation of 2,500 m in the east, down to less than 2,000 m in the west. The Angouran travertine plateau with the Angouran mine camp on top (Fig. 2a) is one of the most prominent and rests unconformably on Miocene pyroclastic rocks.

Geometry and zoning of the ore types

The ore zone at Angouran has a complex geometry. The ores are located in the crest of an open anticlinal structure within the metamorphic basement that plunges eastward at 10 to 20°. The dimensions of the mineralized zone range from some 600 m in length (N-S) to 200 to 400 m in width (Fig. 3). The orebodies are delimited by two major NNW-SSE and NW-SE trending faults and a third NE-SW fault. The up to 200-m-thick Zn carbonate ores, which occur discordantly in the hanging-wall marbles (Fig. 3), overlie a tabular sulfide orebody (Gilg et al. 2006). Smaller bodies of mixed sulfide and carbonate ore occur at the contact between sulfide and nonsulfide zones, as well as within the nonsulfide ores. Both sulfide and carbonate ore types also fill a wide variety of breccias, especially along the three main fault zones that are laterally controlling the deposit. In fact, there is no sulfide ore that does not contain traces of smithsonite mineralization due to the variable degree of carbonatization of the primary ore. One of the most peculiar breccia types, consisting originally of marble clasts cemented by sulfides (sphalerite ≫ galena > pyrite), has been transformed into a mixed sulfide–carbonate mineralization style. Concretionary, vuggy smithsonite (Fig. 2c), ranging in color from pinkish to white (Fig. 2d,e), has completely replaced the former marble clasts. Small concentrations of soft "calamine" ore (Fig. 2g), in which both Zn carbonates and silicates replace patchily the host rock carbonates (Daliran and Borg 2005b), occur along the border of the main deposit. Karstic cavities filled with travertine-like carbonates and stalactites in the marble adjacent to the "oxidized" orebodies have been encountered locally.

Following a descriptive classification by the IZMDC geologists, seven distinct ore types have been distinguished at Angouran (see also Gilg et al. 2003a; Daliran and Borg 2003, 2005b):

- Predominant *hard carbonate ore* (HCO; in close contact with sulfides),
- *Soft carbonate ore* (SCO) with a high clay content, usually overlying the hard carbonate ore,
- Very porous, vuggy *breccia ore* (BO) with clasts of hard carbonate ore,
- Creamy white massive *calamine ore* (rare; CO),
- *Very low grade ore* (VLGO),
- *Sulfide ore* (SO),
- *Mixed sulfide–carbonate ore* (MSO).

Materials and methods

The samples analyzed for this study were taken from drillcore DB 90 and selected outcrops within the Angouran open pit (partly provided by M. Sadeghi). We have also sampled the carbonate host rocks, several travertines, and the waters from thermal springs in the surroundings of the mine. A.E. Annels (SRK) collected for us an extra set of carbonate samples (characterized by letter A- in Table 5). Brief sample descriptions are given in Table 5. Mineral samples were characterized by optical microscopy, X-ray powder diffraction (XRPD, Seifert MZVI automated diffractometer, CuKα radiation), and scanning electron microscopy (SEM, Jeol JSM-5310). Silicates, oxides, and pure elements were used as standards; operating conditions were 15-kV acceleration voltage and 10-μm spot size. Polished thin section (~30 μm thick) of most samples were also examined by cold cathodoluminescence (CL) petrography, utilizing a CITL 8200 Mk3 Cold Cathodoluminescence instrument at the Geologisch-Paläontologisches Institut, Universität Heidelberg (Germany), operating at 23–25-kV voltage and 500–550-μA beam current.

Main-element analyses of selected samples were carried out using energy-dispersive spectroscopy (EDS) mode (Link Analytical 10000, ZAF corrections). Additional chemical analyses of smithsonite were performed using wavelength dispersion spectrometry (full WDS) on a Cameca SX50 electron microprobe (IGAG at the CNR, Rome) operating at 15 kV, 15 nA, and 10-μm spot size. Data were corrected using the PAP program of Pouchou and Pichoir (1991) on the basis of minerals and pure element standards. Ca and Zn carbonates were analyzed for a total of 36 elements using inductively coupled mass spectrometry (ICP-MS) following digestion with aqua regia at 95°C by ACME Analytical Laboratory (Vancouver, Canada).

Fluid inclusion microthermometry was performed at the Geological Survey of Canada (GSC) on a US Geological Survey heating/freezing stage at GSC-Quebec with precision of ±0.2 for ice melting temperatures and ±1°C for homogenization temperatures.

Thermodynamic calculations have been performed using The Geochemist's Workbench® 4.0 (Bethke 2002) and a modified version of the *Thermo2000* database (Cleverley et al. 2003, with $\Delta_f G^0_{1.298}$ of arsenopyrite [FeAsS] from Pokrovski et al. 2002).

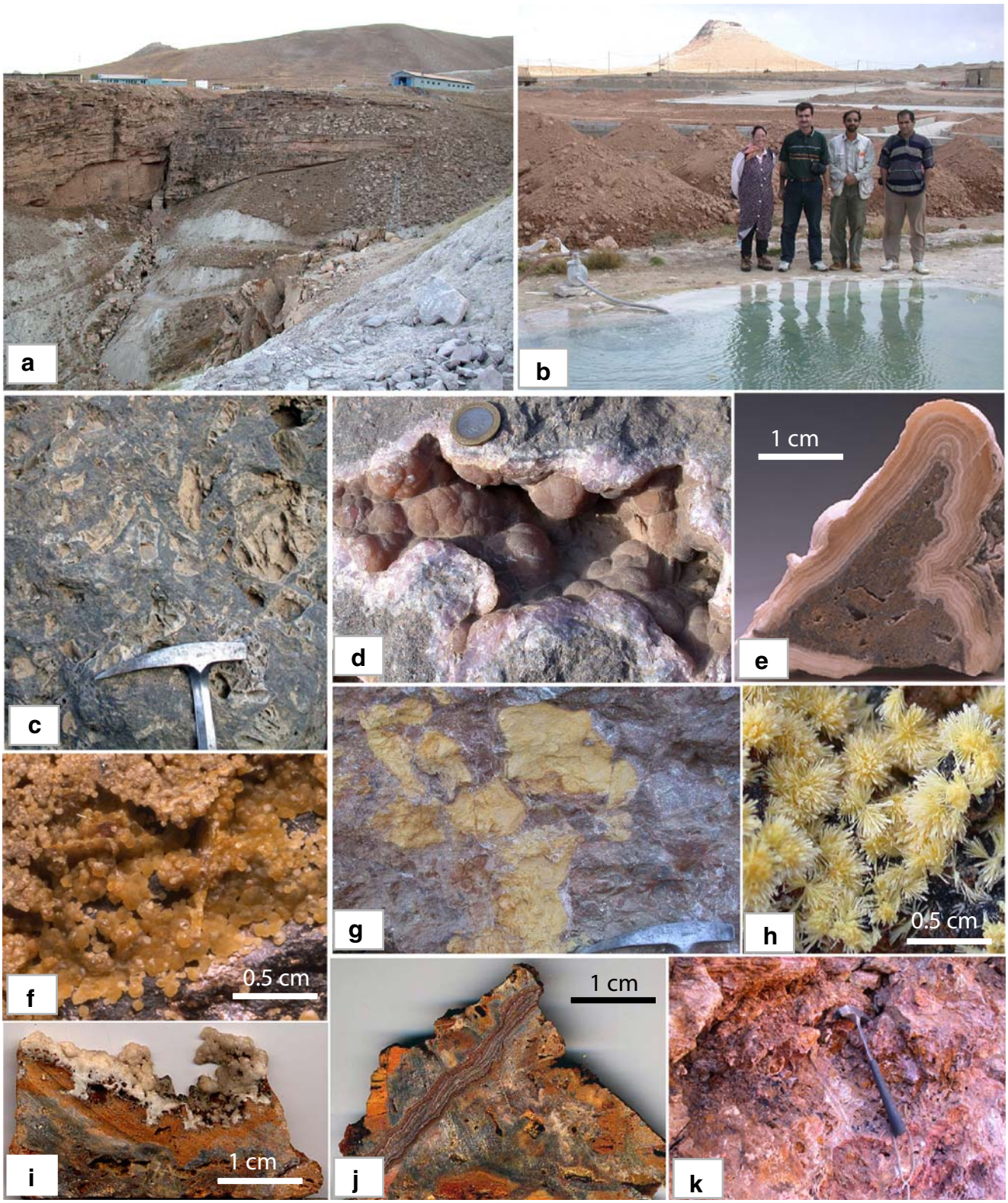

Fig. 2 **a** Angouran mine camp travertine (500 m east of the mine); **b** Ahmadabad hot spring: in the background, the travertine cone of Zendan-e Soleiman; **c** mineralized breccia: former marble clasts (now replaced by concretionary smithsonite), cemented by massive sulfides (stage I carbonate ore); **d** pink colloform smithsonite (Ib) in vug (stage I carbonate ore); **e** colloform smithsonite around a core of hard carbonate (stage I carbonate ore) (ANG B15-A); **f** zoned smithsonite concretions (Ib) growing on sulfide ore (stage I carbonate ore) (ANG B13); **g** soft "calamine" ore; **h** yellow mimetite crystals on oxidized surface; **i** stage I carbonate ore which has undergone oxidation. The white carbonate concretions on the top are replacing former silicates (hemimorphite?) (ANG B15-B2); **j** oxidized stage I carbonate ore crossed by a zoned band of stage II carbonate ore (Sm II) (ANG B15-B1); **k** primary stage I carbonate ore, oxidized on a pit face

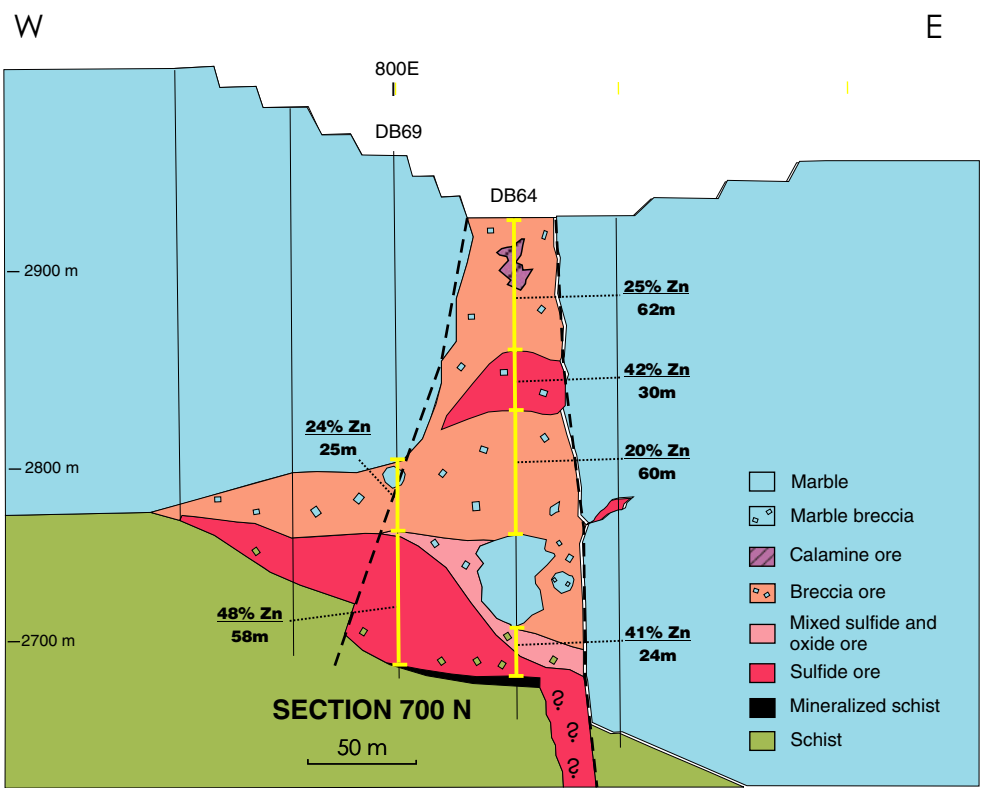

Fig. 3 Geological E–W section through the Angouran orebody; the mixed sulfide and oxide ores display an inverted mushroom shape. Elevation in meters above sea level. Average Zn content is shown for two drill cores

Stable oxygen and carbon isotope ratios of carbonates were determined using an automated on-line device operated in continuous flow mode (Finnigan Gasbench II) and a Finnigan Deltaplus mass spectrometer at the GeoBio-Center, LMU Munich. The carbonate samples were reacted with anhydrous phosphoric acid at 72°C. We used phosphoric acid fractionation factors for the various minerals from Gilg et al. (2003b). The isotope analyses are reported as permil deviations (δ values) from Vienna Standard Mean Ocean Water (VSMOW) for oxygen and Vienna Peedee Belemnite (VPDB) for carbon. The precision of analyses based on repeated measurements of laboratory (LM) and international standards (NBS-18, NBS-19) is about 0.1‰ (1σ).

For Rb–Sr isotopic analysis, carbonate samples were completely dissolved in 14 N HNO_3 and rock samples dissolved in a 5:1 mixture of 24 N HF and 14 N HNO_3. The rock solutions were totally spiked with a mixed ^{87}Rb–^{84}Sr tracer for Rb and Sr concentration analysis by isotope dilution and simultaneous determination of the $^{88}Sr/^{86}Sr$ ratios during the Sr run. All solutions were then dried at 110°C and subsequently rewetted with 3 N HNO_3. Rb and Sr were separated with 3 N HNO_3 using EICHROM Sr resin on 50-µl Teflon columns, following the methods of Horwitz et al. (1991a, b). The first 600 µl of HNO_3 wash of the spiked rock solutions were collected and used for measurement of Rb. Sr was stripped from the columns with 1 ml of H_2O.

For mass spectrometry, Sr was loaded with $TaCl_5$–HF–H_3PO_4 solution (Birck 1986) onto W single filaments. Rb was loaded with DDW onto the evaporation ribbon of a Ta double-filament assemblage. All isotopic measurements were performed on a FINNIGAN MAT 262 solid-source mass spectrometer running in static multicollection mode. Sr isotopic ratios were normalized to $^{86}Sr/^{88}Sr=0.1194$. Repeated static measurements of the NBS 987 standard over the duration of this study yielded an average $^{87}Sr/^{86}Sr$ ratio of 0.71025±2 (2σ mean, n=18). Individual uncertainties (2σ) are given for Rb–Sr elemental concentrations and isotope ratios (Table 5). Total procedure blanks amounted to 30 pg Sr and were found to be negligible with respect to the results. Rb–Sr ages were calculated after Ludwig (2003) using the ISOPLOT/Ex version 3.00 program; errors on the ages are quoted at the 2σ level.

Petrography and paragenesis of nonsulfide mineralization at Angouran

In almost all sulfide ore samples, there is a variable content of Zn carbonates (Gilg et al. 2003a, 2006; Daliran and Borg 2005b). The latter replace former sulfate minerals, marble clasts in the breccias, and sulfides, suggesting that Zn carbonate ore formation has pervasively overprinted the sulfide ore. Zn carbonates occur also (along with minor hemimorphite) as cavity and fracture fill. According to Gilg et al. (2003a), two main paragenetic stages of Zn nonsulfide mineralization can be distinguished, They are

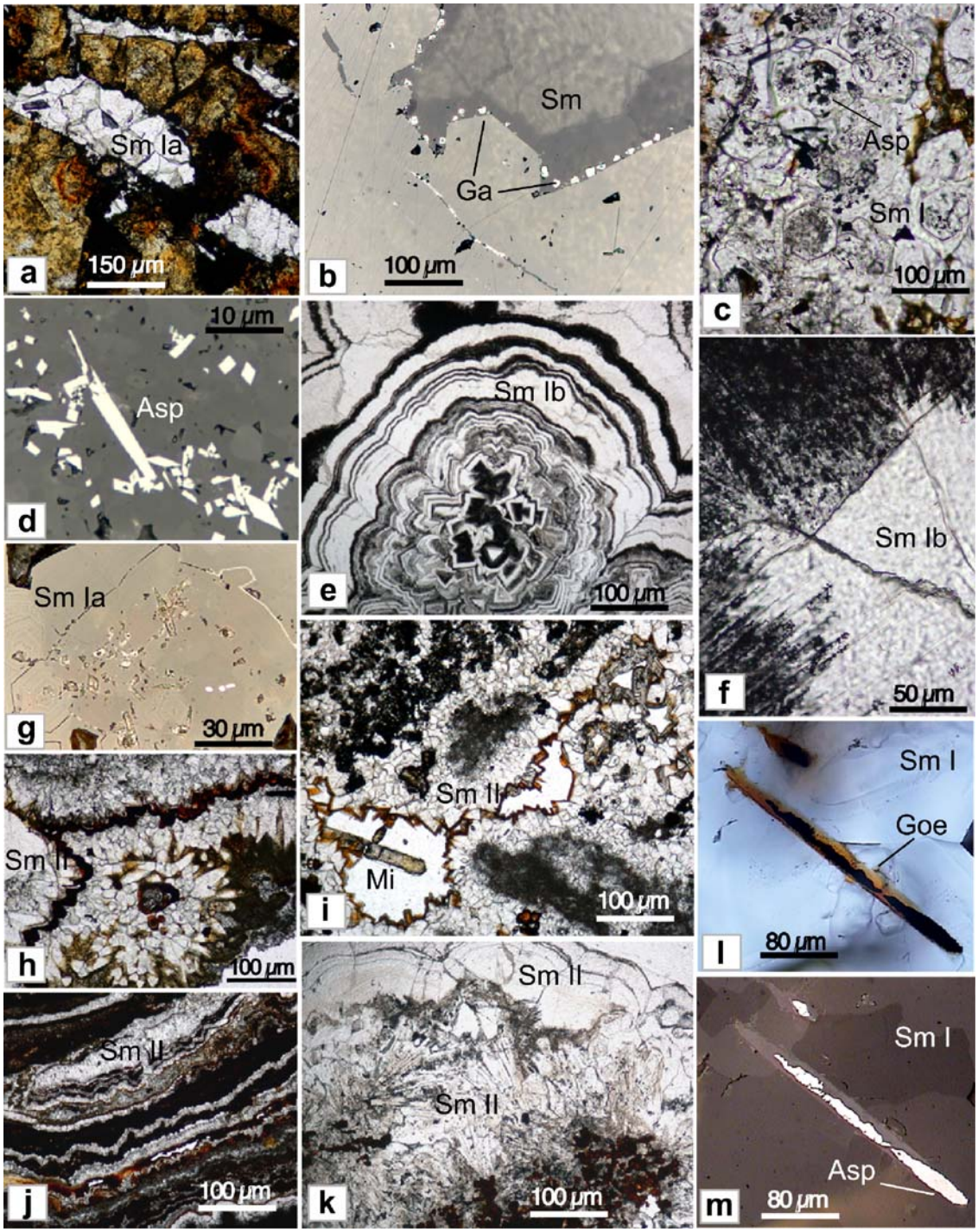

Fig. 4 **a** Tabular ghost minerals (former sulfates) in sphalerite (brown-yellow) ore partly filled with smithsonite Ia (Sm) of stage I carbonates. Transmitted light (ANG B14); **b** newly formed galena (Ga) in cavity (former sulfates) of sulfide ore. Reflected light (ANG B3); **c** stage I carbonate ore with arsenopyrite (Asp) in smithsonite (Sm) and quartz (Qz). Transmitted light (ANG B15B2); **d** arsenopyrite rhombs (Asp) in smithsonite Ia from stage I carbonate ore. Reflected light (ANG B14); **e** colloform zoned smithsonite Ib (Sm) from stage I carbonate ore. Transmitted light (ANG B15-B); **f** enlargement of one of the dark, fluid inclusion-rich bands from **e**. Transmitted light (ANG B15-B); **g** stage I carbonate ore with zoned crystals of smithsonite Ia. Transmitted light (ANG B15-B2); **h** stage II carbonate ore with smithsonite II crystals (Sm) alternating with bands of Fe (hydr)oxides. Transmitted light (ANG B15-B1); **i** stage II carbonate ore with smithsonite II on Fe (hydr)oxides (*black*) and prismatic euhedral mimetite (Mi) in the center. Transmitted light (ANG B15-B1); **j** zoned band of stage II carbonate ore (smithsonite II) with Fe (hydr)oxides and arsenates. Transmitted light (ANG B15-B1); **k** white carbonate crusts of smithsonite II from stage II carbonate ore replacing former silicates (hemimorphite?). Transmitted light (ANG B15-B2); **l** partly oxidized arsenopyrite crystal (Asp) in smithsonite Ia (Sm); *brown patches* correspond to goethite (Goe). Transmitted light (ANG B14); **m** same as **l**. Reflected light

defined as: (1) stage I zinc carbonate ore (partly coexisting with sulfides), (2) stage II zinc carbonate ore (coexisting with oxides). These ore assemblages comprise the various types of smithsonite-dominated "oxide" ores.

The deposition of the different phases of stage I zinc carbonate ore did not directly follow that of the latest Zn sulfides (Fe-poor, honey sphalerite, Gilg et al. 2006). During a hiatus after sulfide mineralization, most of the sulfates (anhydrite and/or barite) were dissolved creating porosity available for Zn carbonate precipitation (Fig. 5). The clear distinction between the nature of the ore fluids depositing the sulfides (Ca–Na–Cl brines of seawater evaporation origin) and the composition (that will be reported later) of the waters depositing the Zn carbonates is evidence for two distinct mineralization processes.

Stage I carbonate ore

Stage I carbonate ore represents the dominant Zn non-sulfide phase in the hard carbonate ore, breccia ore, calamine ore, mixed sulfide–carbonate ore and is also a trace component in almost all examined sulfide ore samples. The texture of the carbonates in the breccia ore is particularly intriguing, as the marble clasts of a sulfide-cemented breccia have been almost completely replaced by pinkish smithsonite concretions with irregular vugs (Fig. 2c). The stage I carbonate ore is dominated by smithsonite I (Fig. 5) that displays a variety of textures from massive to brecciated, botryoidal, and colloform to euhedral dogtooth-shaped, and vuggy to dense (Figs. 2d–f, 4a,e,g, and 6a,b). Stage I carbonate mineralization associated with sulfide ores fills the cavities of former sulfate laths (Fig. 4a) and replaces marble fragments or even primary sulfide ores without apparent oxidation or dissolution of the sulfide minerals (Fig. 2e). The earliest mineral is a peculiar generation of galena in small cubes (Fig. 4b), growing along the border of cavities produced by dissolution of former sulfate minerals (anhydrite, after Gilg et al. 2006, or barite, after Daliran and Borg 2005b). Based on CL imaging, several generations of smithsonite I (Sm Ia, Ib, Ic) could be distinguished. Smithsonite Ia occurs in the former sulfate cavities as zoned, dogtooth-shaped crystals (Fig. 7a). Smithsonite Ib commonly displays a cloudy, dark core with abundant, less than 1-μm-sized fluid inclusions followed by a clear, zoned rim (Figs. 4e,f and 7b,c), with sulfides and quartz on specific growth zones. CL colors of smithsonite Ia are variable from deep red to purple (Fig. 7a), while those of Ib are extremely zoned, grading to bluish varieties (Fig. 7b). Irregular, inclusion-rich bands in smithsonite Ib are strongly luminescent in purple tones (Fig. 7c). A third generation of smithsonite (Ic), strongly purple under CL, is visible in late fillings and as thin veins cutting generations Sm Ia and Ib. There is no apparent correspondence between CL zoning and gross chemical composition of smithsonite, as detected by Götte and Richter (2004). Smithsonite Ia exhibits abundant euhedral, acicular arseno-

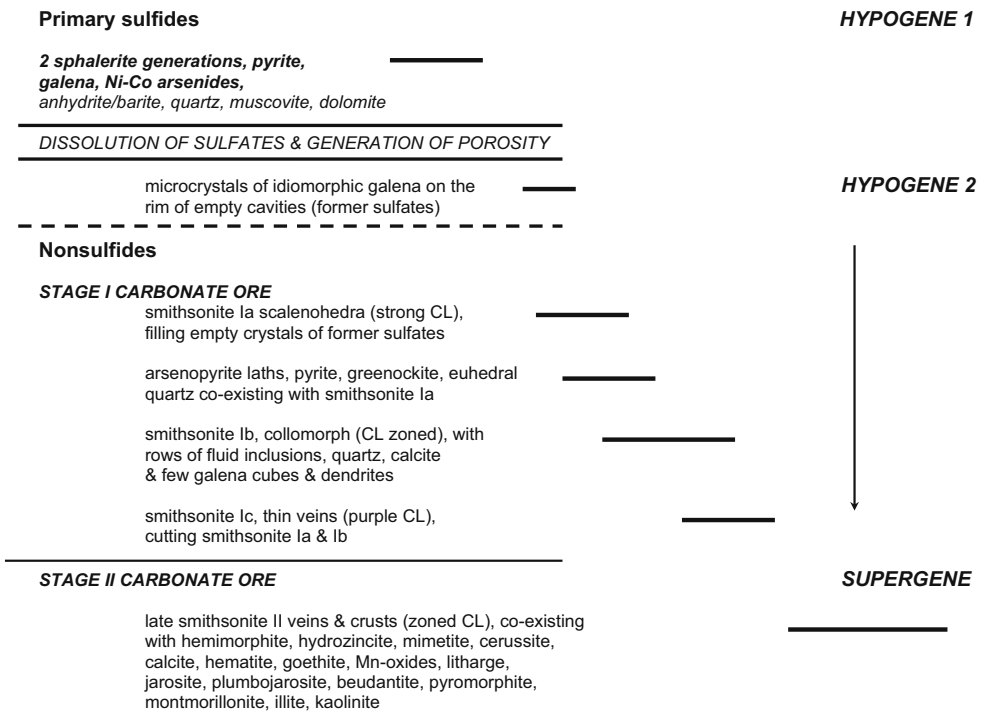

Fig. 5 Paragenesis of sulfide and nonsulfide ores at Angouran

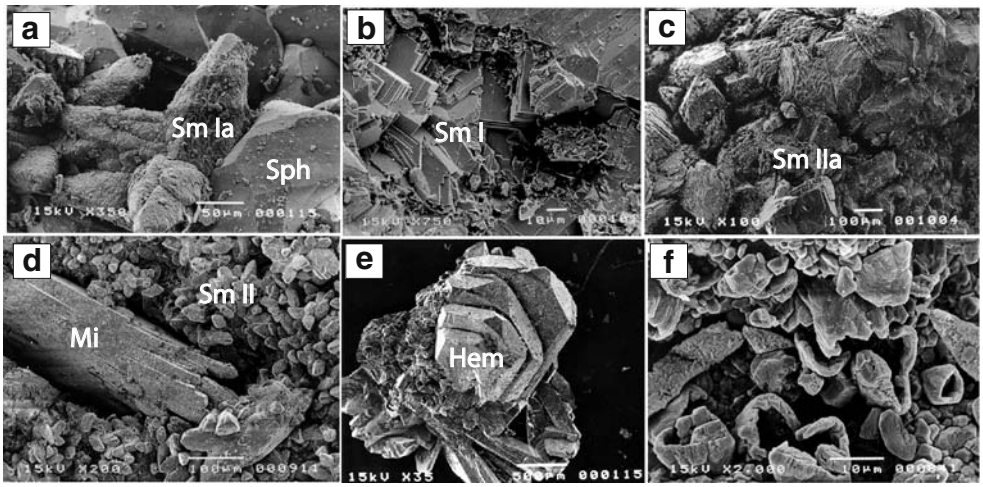

Fig. 6 Scanning electron microscope (SEM) images. **a** Smithsonite I (Sm I) crystals growing in cavities of sphalerite (Sph) ore (stage I carbonate ore) (ANG B3); **b** sparry smithsonite I (Sm I) vein cutting sulfides (stage I carbonate ore) (ANG B3); **c** slightly oxidized smithsonite I crystals (ANG B15B); **d** smithsonite II (Sm II) with mimetite crystal in the middle (ANG B15B); **e** hemimorphite crystals (Hem) in a druse of smithsonite II (ANG B15A); **f** empty Fe (hydr)oxide crusts around dissolved smithsonite (ANG B16)

pyrite inclusions (Fig. 4c,d), and subordinately, euhedral quartz, galena, pyrite, and greenockite crystals (all <5 μm). It is noteworthy that arsenopyrite is not found in the early sulfide ore paragenesis (Gilg et al. 2006). Tiny cubes, as well as dendrites of galena and euhedral quartz crystals (Fig. 4c), are found also in some growth zones of the colloform smithsonite Ib. In some samples, the association smithsonite I-arsenopyrite seems to replace earlier sulfide ores, while in many other areas, direct replacement of the marbles by zebra-textured smithsonite-calcite ore could be observed. The general absence of Fe or Mn oxides or (hydr) oxide minerals and the presence of the sulfide mineral inclusions are the distinguishing features of the stage I carbonate ore.

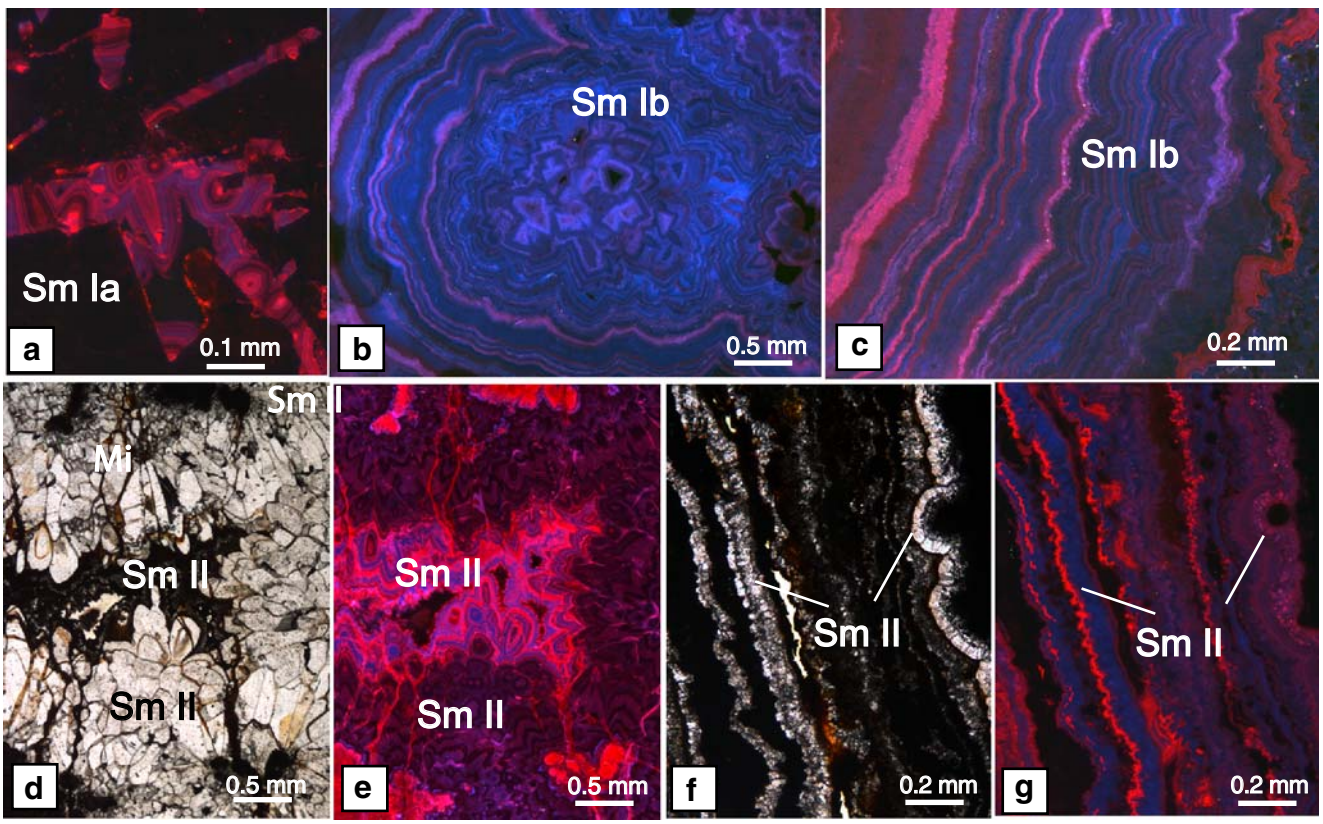

Fig. 7 **a** Former sulfate minerals filled with smithsonite Ia (Sm) of stage I carbonates, zoned under CL (ANG B14-1); **b** colloform zoned smithsonite Ib, showing under CL a *blue* color and a zoned structure (ANG B15-B1); **c** enlargement of image **b**. (CL); **d** two generations of smithsonite II (Sm II) (ANG B15-B1); **e** Same as **d** under CL; **f** Band of smithsonite II (Sm II) alternating with Fe hydr(oxides) (ANG B15-B1); **g** same as **f** under CL

Stage II carbonate ore

Stage II carbonate ore is characterized by the association of newly precipitated smithsonite (smithsonite II, Fig. 5) with hemimorphite, mimetite (and possibly hedyphane), goethite, hematite, various Mn oxides, calcite, and cerussite. It is commonly found in vein fillings as reddish colloform bands with alternating layers of smithsonite, goethite, and mimetite crosscutting stage I carbonate ores (Figs. 2j and 4j), as euhedral crystals in vugs and open fractures (Figs. 4h,i and 6c), or as part of the friable soft carbonate ore. Stage II carbonate ore, however, represents only a very minor percentage of the total amount of carbonate ores.

Stage II Zn carbonates could be distinguished also under CL light due to the much smaller dimension and brighter colors of the smithsonite crystals occurring in the newly formed crosscutting bands (Fig. 7d–g). As a result of supergene oxidation (Fig. 2i–k), the sulfide minerals occurring in the stage I carbonate ore, mainly arsenopyrite and galena, are oxidized (Fig. 4l,m) and transformed into goethite and cerussite, while the host smithsonite I remains fairly unchanged during oxidation. The presence of Fe and Mn oxides (Fig. 6f) and arsenates (Figs. 2h, 4i, and 6d) and the absence of sulfide minerals clearly document the oxidizing conditions during stage II carbonate ore formation. We note that some botryoidal smithsonite crusts (Figs. 2i and 4k) are devoid of both sulfide and oxide inclusions and thus cannot be unambiguously attributed to either one of the two carbonate ore stages. Hemimorphite crystals (Fig. 6e), locally replaced and/or overgrown by smithsonite crusts (smithsonite III?), are mainly associated to the late stages.

We suspect that some stage II smithsonite reflects ground water dissolution of stage I smithsonite in the porous and friable ore mass and its subsequent reprecipitation in the vadose zone.

Calcite

Numerous veins and cements in breccias containing sparry calcite, as well as dogtooth euhedral crystals and travertine-like encrustations in karstic cavities, are found in the host marbles surrounding the Angouran orebody. Calcite was mostly deposited also during the formation of the two Zn carbonate ore stages, associated in prevalence with the stage I carbonate ore.

Fluid inclusions of the stage I carbonate ore

Dogtooth smithsonite crystals from the stage I carbonate ore generally show cloudy cores with primary, submicrometer-sized fluid inclusions that appear to be monophase. Rare, slightly larger (6–12 μm) monophase liquid-only inclusions are found isolated in the crystals or along growth zones. Formation temperatures for these monophase inclusions are estimated to be less than 70°C or even less than 50°C (Roedder 1984). Overheating to about 350°C caused stretching of the monophase inclusions and formation of a small vapor bubble. Thus ice melting in the presence of vapor could be measured in these inclusions. The few microthermometric results with ice melting temperatures ranging from −0.8 to −1.8°C (n=3) show a significantly lower salinity of 1.4–3.0 wt.% NaCl equivalent (and formation temperature) compared to the fluids related to sulfide ores (23–25 wt.% total dissolved solids; Gilg et al. 2006).

Geochemistry

Main and trace elements

Primary sulfide ores are characterized by a very high Zn (>35 wt.%) and generally low Pb content (<3 wt.%, Gilg et al. 2006; Table 1). Conversely, the Zn content of "oxide" ores is more variable, typically <40 wt.% in calamine ore, hard carbonate ore, breccia ore, and <30 wt.% in soft carbonate ore and very low grade ore (Fig. 3). Pb contents in "oxide" ores (~5–7 wt.%) are generally higher than in the primary sulfide ores. Table 1 lists the average trace element composition of 21 sulfide and "oxide" bulk ore

Table 2 Selected trace element concentration (parts per million) of some Angouran smithsonite samples

Sample	Cr	Mn	Co	Ni	Cu	As	Ag	Cd	Sb	Pb	Au (ppb)
ANG B3-S Stage I	b.d.	632	201	259	3	9	b.d.	5	3	668	2
ANG B13-A Stage I	b.d.	110	240	216	9	68	b.d.	259	11	1234	3
ANG B13-R Stage I	b.d.	609	857	1425	81	27	b.d.	159	7	1146	7
ANG B14 Stage I	1	198	261	366	2	26	b.d.	142	4	2251	1
ANG B15 Stage I	b.d.	235	153	146	6	115	1	517	4	2268	28
ANG B15-A Stage I	b.d.	52	101	97	43	124	b.d.	2400	b.d.	4877	6
ANG B15-B2 Stage II	b.d.	22	186	260	24	663	1	3500	13	4572	4
AA 34 Stage II	15	610	721	1057	27	568	18	837	11.7	3532	1.8

b.d. below detection limit

samples, which are dominated by stage I carbonate ores (Teck Cominco, average assay data). Whereas the sulfide ores reveal high Ag, As, Sb, Hg, Co, and Ni contents and low Cu and Mn, the "oxide" ores are enriched in As (6,100 ppm), Sb (570 ppm), and Mn (750 ppm), and depleted in Ag (35 ppm).

The trace element composition of a few bulk smithsonite samples, comprising both stage I and stage II Zn carbonate ores, is shown in Table 2. Stage I Zn carbonate ore, both as smithsonite concretions and veins cutting primary sulfides, has variable Mn (from 50 to 630 ppm) and Pb (from 660 to 4,800 ppm) contents. As is quite low (from 9 to 124 ppm). Stage II Zn carbonate ore has a much higher As content (560–660 ppm). All samples have elevated, although variable Ni and Co contents (Ni from 97 to 1,400 ppm and Co from 100 to 850 ppm). Ni and Co are locally enriched compared to the average values measured in sulfide ores (Gilg et al. 2006), where these elements occur as tiny inclusions of Ni and Co arsenides in quartz.

Microanalyses of smithsonite samples, belonging to both the stage I and stage II Zn carbonate ores, have been carried out also by EDS and WDS analysis (Table 3). The results for the stage I smithsonite samples show only some slight differences in Fe and Mn, with pink and orange varieties having the higher contents. In the stage II samples, the Fe content can be higher than 2 wt.%, while Mn is absent. In the yellow SCO, MnO can reach 0.5 wt.%, together with PbO values around 1.2 wt.%.

Selected trace element data (As, Zn, Pb, Mn, Fe, Sr, Cd, Ba, Ni, Co) for various unmineralized carbonate rocks (marbles, limestones, travertines) are given in Table 4. Compared to the chemical composition of the mineralized marble clasts contained in the sulfide and carbonate ore breccias, the unmineralized carbonate rocks have generally very low metal contents (Zn<30 ppm, Pb<4 ppm, Ni<6 ppm, Co<1 ppm, As<20 ppm, and Cd<1 ppm in the basement marbles and in the Qom limestone). The Qom limestone is only slightly enriched in Cu, Ba, and As compared to the marbles. Conversely, the mineralized marble clasts (both calcitic and dolomitic) are enriched in Zn, Pb, Ni, Co, As, and Cd.

All Quaternary travertine samples (Angouran mine camp, Taxt-e Soleiman, and Zendan-e Soleiman) are characterized by relatively high As and Ba contents (Table 4). The samples from the Angouran mine camp travertine are strongly enriched in Zn (440–1,320 ppm), Cd (1–8 ppm), and Ni (9–14 ppm), as compared to the travertines from Takht-e Soleiman and Zendan-e Soleiman. Similar values have been observed in vein carbonates from the open pit area and in the carbonates from small solution cavities occurring in the DB 90 drill core. Both types of carbonates have Zn values varying between 200 and 2,800 ppm and Pb values ranging from 80 to 970 ppm. As (maximum values around 150–350 ppm), Mn, Ni, Co, and Cd are also enriched in these samples.

C, O, and H isotope data

Carbon and oxygen isotope data of smithsonite, cerussite, and calcite from the Angouran mine and adjacent areas and oxygen and hydrogen isotope data of spring waters are presented in Tables 5 and 6.

Smithsonite from stage I carbonate ore displays variable $\delta^{18}O_{VSMOW}$ values ranging from 18.3 to 23.6‰ (n=21), while the carbon isotope composition is fairly constant and unusually high (+3.2 to +6.0‰) with an average value of 4.9‰±0.8‰ (1σ). In contrast, the smithsonite from stage II carbonate ores shows a much smaller range of $\delta^{18}O_{VSMOW}$ values from 24.3 to 24.9‰ but a considerable spread towards lower $\delta^{13}C_{VPDB}$ values (−0.8 to 4.6‰). Cerussite shows C–O isotope values similar to stage II carbonate ores, with relatively constant $\delta^{18}O$ (12.7–15.1‰) but highly variable $\delta^{13}C$ (−11.2 to +1.9‰). Such C–O isotope patterns (Fig. 8) are quite characteristic for supergene carbonate minerals in sulfide oxidation zones (Gilg and Boni 2004a, b; Gilg et al. 2007), meteoric carbonate cements (e.g., Lohmann 1988), and pedogenic carbonates (e.g., Salomons and Mook 1986; Talma and Netterberg 1983). The observed ^{13}C enrichments are characteristic for travertine-depositing systems (e.g., Turi 1986; Minissale et al. 2002).

Sparry vein calcite, euhedral crystals in the carbonate ore, and travertine-like cavity fillings in and around the ore bodies at Angouran have variable $\delta^{18}O_{VSMOW}$ values ranging from 15.6 to 21.7‰ and $\delta^{13}C_{VPDB}$ values from −1.3 to +6.1‰ (Table 5, Fig. 9). The carbon and oxygen isotope values are negatively correlated. We interpret this isotope variation as indicative of calcite precipitation from a mixture of two isotopically distinct fluids. The majority of calcite samples with low $\delta^{18}O_{VSMOW}$ (17±2‰) and high $\delta^{13}C_{VPDB}$ values (5±1‰) are related to precipitation from hydrothermal, travertine-depositing solutions. Few calcite samples with heavy oxygen and light carbon isotope values ($\delta^{18}O_{VSMOW}$= 21±1‰; $\delta^{13}C_{VPBD}$=−1±1‰) were formed from the second end member fluid, corresponding to cold groundwater.

The Angouran marble samples exhibit a large spread in carbon (0.5–4.6‰) and oxygen isotope values (17.7–27.1‰), which are negatively correlated (Table 5, Fig. 9). The isotope composition of the least altered marble samples ($\delta^{13}C_{VPBD}$=1.3±0.5‰; $\delta^{18}O_{VSMOW}$=26±1‰) is consistent with a marine origin and a rather limited isotope exchange during diagenesis and greenschist-facies metamorphism. Marble clasts from mineralized and some barren but calcite-veined breccias display a distinct alteration trend towards lower oxygen and higher carbon isotope values. The isotope composition of the altered marble overlaps

Table 3 Chemical analyses (EDS–WDS) of representative Angouran smithsonite samples (mean of five- to ten-point analyses)

Sample	ANG B3-1 Stage I	ANG B3-2 Stage I	ANG B13-A Stage I	ANG B13-R Stage I	ANG B14-1 Stage I	ANG B14-2 Stage I	ANG B14-3 Stage I	ANG B15-1 Stage I	ANG B15-3 Stage I	ANG B15A-B Stage I	ANG B15A-R Stage I	ANG B15A-M Stage I	ANG B15B Stage I	ANG B15-B1 Stage II[a]	ANG B18 Stage II[a]	ANG B20 Stage II[a]
ZnO	62.33	62.37	62.85	62.34	63.34	63.02	64.35	63.02	62.51	62.12	62.83	62.33	60.97	62.11	63.51	54.64
CaO	0.25	0.34	0.57	1.39	0.84	0.39	0.21	1.02	0.84	0.98	0.85	0.25	0.25	1.46		
MgO					0.38	0.68			0.34				0.27			
FeO	1.87	1.64	1.38	0.56		0.36		0.10	0.68		0.69	1.87	2.80			9.63
MnO	0.36	0.48		0.16						0.68		0.36	0.07		0.53	
CdO										0.64	0.13		0.71	0.55		
PbO				0.56				0.56		0.58				0.21	1.23	0.49
CO_2[b]	35.42	35.45	35.43	35.51	35.48	35.50	35.12	35.21	35.40	35.27	35.26	35.42	35.61	35.12	35.07	35.68
Sum	100.23	100.28	100.23	100.52	100.04	99.95	99.68	99.91	99.77	100.27	99.76	100.23	100.68	99.45	100.34	100.44
Structural formulae on the basis of 6 O																
Zn	1.91	1.906	1.921	1.902	1.934	1.923	1.985	1.930	1.91	1.91	1.930	1.91	1.86	1.92	1.96	1.66
Ca	0.01	0.015	0.025	0.062	0.037	0.017	0.009	0.05	0.04	0.04	0.04	0.01	0.011	0.065		
Mg					0.023	0.042			0.02				0.017			
Fe	0.07	0.057	0.048	0.019		0.012			0.02		0.03	0.65	0.097			0.331
Mn	0.01	0.017		0.006						0.02		0.01	0.002		0.017	
Cd										0.01			0.014	0.011		
Pb				0.006				0.01		0.01				0.002	0.014	0.005
C	2.000	2.000	2.000	2.000	2.000	2.000	2.000	2.000	2.000	2.000	2.000	2.000	2.000	2.000	2.000	2.000

See text for sample description.
[a] Traces of Fe oxides and cerussite
[b] Calculated from stoichiometry

Table 4 Minor and trace elements concentration in selected Angouran Ca(-Mg) carbonate samples

Samples	Mn wt.%	Fe	V ppm	Cr	Co	Ni	Cu	Zn	As	Sr	Cd	Sb	Ba	La	Pb	Au ppb
AA 1 travertine (Ang mine camp)	0.01	0.12	3	5	b.d.	14	2	448	133	274	1	b.d.	26	b.d.	6	b.d.
AA 2 travertine (Ang mine camp)	0.01	0.2	5	6	2	9	5	1327	115	188	8	1	29	2	60	b.d.
AA 3 travert. (Taxt-e Soleiman)	0.01	0.03	1	b.d.	b.d.	2	b.d.	8	192	461	b.d.	b.d.	14	b.d.	1	b.d.
AA 5 travert. (Zendan-e Soleiman	0.09	0.22	4	3	b.d.	5	2	17	258	273	b.d.	b.d.	87	b.d.	6	b.d.
AA 6 marble	0.13	0.41	3	8	b.d.	6	1	4	6	243	b.d.	b.d.	11	4	4	b.d.
AA 7 marble	0.01	0.04	6	b.d.	b.d.	3	b.d.	15	1	193	b.d.	b.d.	2	b.d.	2	b.d.
AA 8 Qom limestone	0.07	0.28	4	3	b.d.	4	6	23	20	80	b.d.	4	60	b.d.	3	b.d.
AA 12 sparry calcite	0.12	0.18	6	b.d.	b.d.	3	1	440	12	136	479	6	5	38	689	b.d.
ANG B3 C dol. marble clast in sulfides	0.01	1.00	15	1	68	131	1	9980	7	18	3	b.d.	2	b.d.	42	5
ANG B6 marble clast in carbonate ore	0.10	b.d.	10	3	157	91	6	9991	130	47	420	43	b.d.	6	3155	2
ANG B9 marble clast in sulfide ore	b.d.	b.d.	2	b.d.	7	9	5	975	105	298	213	141	b.d.	3	2004	4
A1-1 calcite in vug DB90	0.06	0.13	7	b.d.	32	5	7	911	39	31	32	3	16	3	905	5
A1-2 calcite in vug DB90	0.01	0.02	5	b.d.	1	3	3	645	14	17	102	b.d.	2	3	977	4
A1-3 calcite in vug DB90	0.02	0.08	3	b.d.	6	4	5	793	26	50	9	b.d.	9	1	390	7
A1-4 calcite in vug DB90	0.01	0.02	4	b.d.	2	1	2	361	7	16	5	b.d.	5	b.d.	112	2
A1-5 calcite in vug DB90	0.05	0.22	12	b.d.	17	4	8	614	55	11	25	4	10	6	793	3
A2 lamin. marble	0.03	0.05	38	2	b.d.	3	15	109	14	94	b.d.	3	1	1	149	1
A3 marble	0.01	0.11	22	1	b.d.	34	7	62	7	149	b.d.	b.d.	b.d.	b.d.	89	8
A5-1 marble clast	0.02	0.09	7	2	3	14	6	603	26	69	47	25	1	6	886	5
A5-2 red vein calcite	0.04	0.1	17	2	12	16	14	1767	61	46	126	61	1	7	2170	2
A6-1 marble clast	0.02	0.07	9	2	b.d.	2	9	67	8	105	b.d.	b.d.	2	b.d.	33	12
A6-2 red calcite	0.07	0.37	14	11	b.d.	335	44	319	36	44	b.d.	7	3	b.d.	31	6
A7-1 vein calcite open pit	0.04	0.01	4	b.d.	b.d.	b.d.	b.d.	39	2	293	b.d.	1	1	b.d.	14	1
A7-2 vein calcite open pit	0.03	0.04	4	b.d.	b.d.	b.d.	5	207	6	177	b.d.	11	1	b.d.	81	1
A7-3 vein calcite open pit	0.02	0.26	4	3	2	4	18	1014	150	117	16	81	1	b.d.	733	1
A7-4 vein calcite open pit	0.01	0.23	3	7	2	224	14	2817	357	45	9	60	1	b.d.	333	4
A7-5 vein calcite open pit	0.04	0.03	4	b.d.	b.d.	3	6	232	15	172	b.d.	b.d.	9	b.d.	18	2

b.d. below detection limit

with the isotope composition of hydrothermal calcite and hypogene smithsonite.

Travertine samples from Zendan-e Soleiman, Taxt-e Soleiman, and the Angouran mine camp travertine have very similar oxygen isotope compositions (20.1–22.4‰; Table 5) and display the characteristic ^{13}C enrichment ($\delta^{13}C_{VPBD}$=3.3–11.3‰) of thermogenic travertine (Pentecost 2005). The high C isotope values in thermogenic travertine are generally explained by high-temperature, contact-metamorphic decarbonatization of marine carbonates and deposition of carbonate at the surface at much lower temperatures, usually below 100°C (Turi 1986; Pentecost 2005). Our carbon isotope value for the Zendan-e Soleiman travertine (11.3‰) is broadly consistent with the isotope data (8.7–10.8‰) reported in Savelli and Wedepohl (1969). We note that the Angouran mine camp travertines have carbon isotope values of 3.3–5.4‰, which are similar to carbon isotope values of stage I smithsonite and of the calcite in vugs or fissures and travertine-like carbonate karst infills around and in the Angouran ore body (Fig. 9).

Hydrogen and oxygen isotope compositions of water from several cold springs (<10°C) close to the Angouran Zn–Pb deposit and from hot springs (18–38°C) from the Taxt-e Soleiman travertine-depositing geothermal field (Table 6) are homogeneous with $\delta^{18}O_{VSMOW}$ of −9.9± 0.1‰ and δD_{VSMOW} of −60.5±1.0‰. We suggest that the hot waters emanating in the Taxt-e Soleiman–Ahmadabad geothermal area (~2,140–2,240 m above sea level) are mainly derived from the easterly mountain ranges (>2,500–3,580 m a.s.l.) that host the Angouran deposit. The meteoric waters are characterized by a strong deuterium excess parameter of +20‰, which is also reported from several areas in the Zagros belt (e.g., Moser and Stichler 1980; Farpoor et al. 2004) and from other areas in the Eastern Mediterranean and Middle East (e.g., Gat and Carmi 1970; Gat and Dansgaard 1972). Such high deuterium excess values in meteoric waters are considered to be related to evaporation of seawater under low-humidity conditions (Gat and Carmi 1970). Slightly heavier hydrogen and oxygen isotope compositions are found in cold waters from

Table 5 Carbon, oxygen, and strontium isotope compositions of Ca, Zn, and Pb carbonate samples

Sample No	Location	Description	Mineral	$\delta^{13}C_{VPDB}$	$\delta^{18}O_{VSMOW}$	$^{87}Sr/^{86}Sr$ $\pm 2\sigma$
Stage I carbonate ore						
ANG B15A-B	OP2930,700E–1000N	HCO, concr. ,white, core	sm	4.95	18.33	0.70865±2
ANG B15A-R	OP2930,700E–1000N	HCO, concr., pink, rim	sm	5.09	21.44	0.70821±1
ANG B15B-G	OP2930,700E–1000N	HCO, concr., gray crystals	sm	5.51	23.58	
ANG B15B1-A	OP2930,700E–1000N	HCO, vein with oxidized asp	sm	4.19	20.76	
ANG B15B1-B	OP2930,700E–1000N	HCO, vein with oxidized asp	sm	4.89	21.89	
ANG B15B1-C	OP2930,700E–1000N	HCO, matrix with asp	sm	5.70	20.41	
ANG B15B1-D	OP2930,700E–1000N	HCO, matrix with asp	sm	5.43	22.26	
ANG B15-1	OP2930,700E–1000N	HCO, concr., light (gray-pink)	sm	5.91	21.00	
ANG B15-3	OP2930,700E–1000N	HCO, reddish concr.	sm	5.86	20.65	
ANG B15A-M	OP2930,700E–1000N	HCO, massive, brown, with asp	sm	4.74	20.29	
ANG B3-1	DB90-200 m	SO, concr., pink, rim	sm	4.33	18.87	0.70863±1
ANG B3-2	DB90-200 m	SO, concr., white, core	sm	4.60	21.02	
ANG B13R	OP2930,870E–1070N	MSO, concr., pink	sm	4.25	20.45	
ANG B13A	OP2930,870E–1070N	MSO, concr., orange	sm	4.74	21.73	
ANG B14-1	OP2960,570E–980N	SO, white concr.	sm	6.00	20.59	
ANG B14-2	OP2960,570E–980N	SO, geodic-type matrix	sm	5.84	21.26	
AA0	OP2930,870E–1070N	MSO, pink concr.	sm	4.32	20.99	
AA37B	OP2930,870E–1070N	MSO, pink concr. core	sm	4.24	19.42	
AA37A	OP2930,870E–1070N	MSO, pink concr., rim	sm	3.21	22.71	
AT-1A	DB98-18.6 m	BO, laminated, brown	sm	5.83	22.16	
AT-7A	OP-Teck Cominco	SO, massive vug infill, white	sm	3.96	20.51	
Stage II carbonate ore						
ANG B15B-B	OP2930,700E–1000N	HCO, concr., white sm on Fe oxides	sm II	4.62	24.92	0.70824±3
AT-3A	DB98-97.0 m	BO, breccia cement, brown	sm II	3.08	24.33	
AT-4A	DB98-113.9 m	MSO, brecciated, laminated, brown,	sm II ± hm	−0.78	24.93	0.70895±1
AA-10	OP2910,750E–990N	MSO, crystal in vug	ce	−1.41	13.46	
AA-9	OP2910,750E–990N	SCO, black, massive	ce	−11.15	12.70	
AA36B	OP2910,750E–990N	SCO, white, massive with Fe oxides	ce	1.93	14.64	
AA36A	OP2910,750E–990N	SCO, dark, massive with Fe oxides	ce	−2.61	15.09	
ANG B20	OP2940,880E–1040N	SCO, red fine-grained matrix + Fe (hydr)ox+qz	sm + cc	2.12	18.53	
ANG B18	OP2940,850E–1090N	SCO, green fine-grained matrix	cc + sm	1.88	17.23	
ANG B18	OP2940,850E–1090N	SCO, green fine-grained matrix	cc + sm	2.12	16.32	
Ca carbonates, marbles, and travertines						
AT-2A	DB89-50.8 m	BO, sparry, vein	cc + hm + sm	5.62	18.33	0.70851±1
ANG B10-1	DB90-20 m	BO, white sparry, vug filling	cc	5.11	16.84	
ANG B10-2	DB90-20 m	BO, dark sparry, vug filling	cc	5.16	18.30	
ANG B11-A	OP2930 near DB90	sparry cc in breccia	cc	2.70	19.53	
ANG B19-A	OP2940,890E–1060N	SCO, white cc with goe	cc	2.23	20.11	
ANG B7-1	DB90-94 m	Travertine-like banded white cc in marble	cc	5.13	16.94	
ANG B7-2	DB90-94 m	Travertine-like banded reddish cc in marble	cc	5.05	15.60	
A7-1	OP2970	Fissural vein, white cc	cc	5.91	16.13	
A7-2	OP2970	Fissural vein, yellow to green cc	cc	6.12	16.69	
A7-3	OP2970	Fissural vein, orange cc	cc	4.11	16.68	
A7-4	OP2970	Fissural vein, red cc	cc	4.93	17.78	
A7-5	OP2970	Fissural vein, brown cc	cc	1.04	18.72	
A1-1	DB62-31.5 m	Dark brown sparry, vug filling	cc	3.30	19.09	
A1-2	DB62-31.5 m	White sparry, vug filling	cc	3.63	18.57	
A1-3	DB62-31.5 m	Orange, vug filling	cc	−0.30	20.69	
A1-4	DB62-31.5 m	Colorless vug filling	cc	4.73	19.45	
A1-5	DB62-31.5 m	Light brown, vug filling	cc	−1.32	21.67	

Table 5 (continued)

Sample No	Location	Description	Mineral	$\delta^{13}C_{VPDB}$	$\delta^{18}O_{VSMOW}$	$^{87}Sr/^{86}Sr$ $\pm 2\sigma$
A5-2	DB84-58.1 m	Red cc vein in breccia	cc	5.06	18.44	
A6-2	DB84-107.5 m	Red, fine-grained cc in breccia	cc	2.01	21.46	
AA12	Open pit	Sparry cc	cc	2.40	18.14	
A5-1	DB84-58.1 m	Gray clast from marble breccia	Marble	4.53	19.30	
A6-1	DB84-107.5 m	Clast from marble breccia	Marble	1.74	23.68	
ANG B3	DB90-200 m	Dolomite marble clast in sulfide ore	Marble	3.51	21.19	0.70836±1
ANG B6A	DB90-104.5 m	Dark gray marble clast in breccia	Marble	3.30	21.02	
ANG B9A	DB90-34.5 m	Marble clast in breccia ore	Marble	1.51	27.09	0.70746±1
ANG B9B	DB90-34.5 m	Marble clast in breccia ore	Marble	2.87	24.00	0.70846±1
ANG B8A	DB90-40 m	Marble clast in hard carbonate ore	Marble	3.61	18.81	0.70820±1
ANG B8B	DB90-40 m	Marble clast in hard carbonate ore	Marble	4.58	17.69	
ANG B6B	DB90-104.5 m	Marble clast in breccia	Marble	2.50	21.14	
A3	DB62-135 m	Marble	Marble	0.83	26.07	
A2-1	DB62-116.8 m	Laminated marble	Marble	2.87	26.46	
AA7	Outcrop, far from ores	Marble	Marble	0.84	24.15	
AA-14a	OP	Marble at contact to calamine ore	Marble	0.54	26.82	
AA6	Outcrop, far from ores	Footwall marble layer in schists	Marble	−3.94	16.03	
AA8	Outcrop, far from ores	Qom limestone	Limestone	−1.85	21.11	
AA1	Ang mine camp, bottom		Travertine	5.37	20.08	
AA2	Ang mine camp, top		Travertine	3.31	21.34	
AA3	Zendan-e Soleiman		Travertine	11.31	20.74	
AA5	Taxt-e Soleiman		Travertine	4.79	22.43	

sm Smithsonite, ce cerussite, cc calcite, qz quartz, asp arsenopyrite, chl chlorite, ms muscovite, goe goethite, hm hematite, *concr* concretion, *OP* open pit, *DB90* drill core, *DB62* drill core, *HCO* hard carbonate ore, *SO* sulfide ore, *BO* breccia ore, *MSO* mixed sulfide-carbonate ore, *SCO* soft carbonate ore.

the Ayagh Bolaghi spring at the Zarshuran As mine and in the Amirabad cold spring.

Rb–Sr isotope data

Sr and Rb–Sr isotope data for smithsonite and calcite from the mineralization, host marbles, and two samples of metamorphic host schists of the Angouran deposit have been obtained. The carbonate minerals and host marbles have unradiogenic $^{87}Sr/^{86}Sr$ ratios between 0.7074 and 0.7089 (Table 5). However, vein calcite and stage I smithsonite samples are mostly slightly more radiogenic than the (possibly hydrothermally altered) marble fragments occurring in the breccia and hard carbonate ore types. One sample of stage II smithsonite is even more radiogenic, with $^{87}Sr/^{86}Sr=0.70895$. The two analyzed schist samples show low $^{87}Rb/^{86}Sr$ ratios of about 1.24 and 7.58 (Table 7), and their $^{87}Sr/^{86}Sr$ ratios are 0.70888 and 0.71104, respectively. Stage II smithsonite samples are even more radiogenic. In the $^{87}Sr/^{86}Sr$ vs $^{87}Rb/^{86}Sr$ space, the slope of a straight line through the two schist samples corresponds to an early Miocene two-point Rb–Sr isochron age of 24.0±0.4 Ma that, if interpreted as a two-point isochron with geochronological significance, most likely records a metamorphic recrystallization age.

Table 6 Hydrogen and oxygen isotope data of waters from hot and cold springs in the Angouran region

	Temp (°C)	Elevation (m a.s.l.)	$\delta^{18}O$ (‰)	$\delta^{2}H$ (‰)	Deuterium Excess (‰)
Soulakhan spring	<10		−10.09	−60.5	20.2
Explosive storage spring	<10	2380	−9.84	−59.7	19
Covered spring (tap water mine camp)	<10	2680	−10.07	−60.2	20.4
Amirabad spring	<10	2389	−9.32	−55.1	19.5
Ahmadabad 1 spring	37.8	2142	−10.15	−61.3	19.9
Ahmadabad 2 spring	28.5	2139	−10.01	−61.5	18.6
Taxt-e Soleiman	18.3	2235	−9.85	−60.2	18.6
Ayagh Bolaghi spring-Zarshuran	8		−9.42	−56.3	19.1

Thermodynamic calculations

Figure 10 depicts the results of thermodynamic calculations performed to explore the geochemical conditions responsible

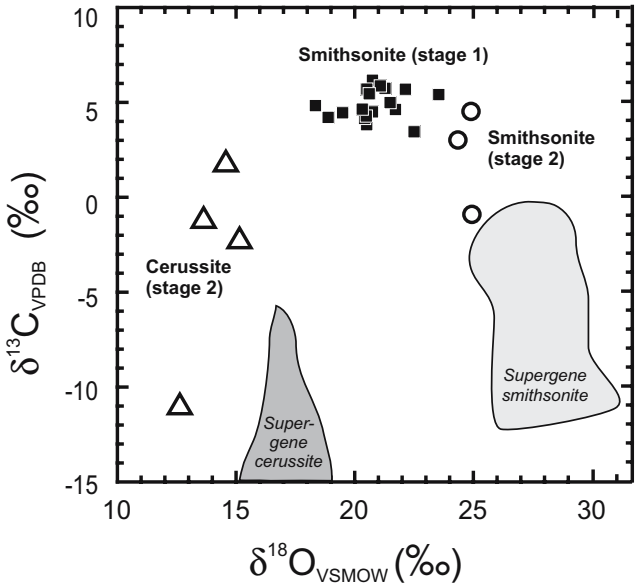

Fig. 8 Stable oxygen and carbon isotope compositions of smithsonite and cerussite from Angouran. The *shaded* fields of supergene smithsonite and cerussite from Gilg et al. (2007) are shown for comparison. Note that the majority of supergene cerussite samples in Gilg et al. (2007) have $\delta^{13}C$ values of less than −15‰. Stage 1 smithsonite samples have an unusual pattern in this δ–δ plot with constant and heavy carbon isotope values and variable oxygen isotope values that is interpreted as indicating a hydrothermal travertine-

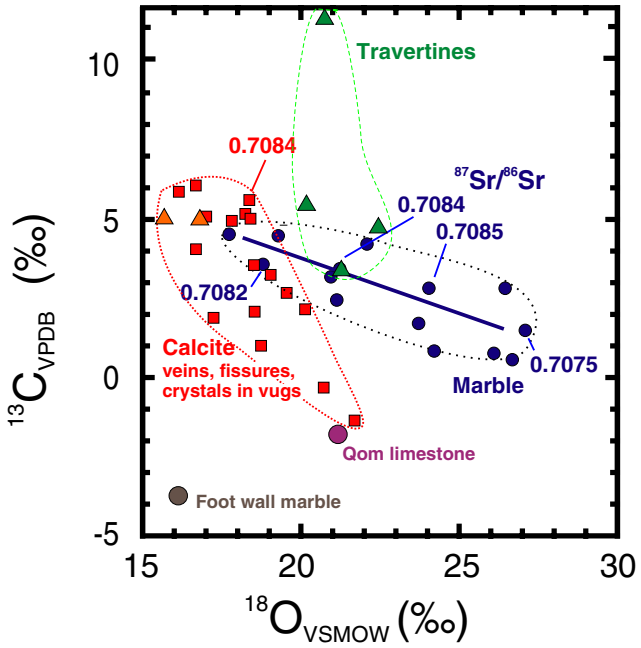

Fig. 9 Stable oxygen and carbon isotope composition of Ca carbonates from veins, fissures, and crystals in karstic vugs in and around the Angouran ore bodies (*red squares*), travertine-like encrustations in similar cavities (*orange triangles*), travertines in the area (*green triangles*), Angouran marble from mineralized breccias and outside the mineralized zone (*blue dots*), foot wall marble (*brown dot*), and Miocene Qom limestone (*violet dot*). Strontium isotope composition of selected marble samples is indicated. The *blue arrow* shows a trend of increasing carbon and strontium and decreasing oxygen isotope ratios as a consequence of increasing hydrothermal alteration

for the observed mineral paragenesis of stage I carbonate ores (smithsonite + quartz + arsenopyrite + galena ± sphalerite). The diagram in Fig. 10a shows the stability field of smithsonite + quartz relative to willemite, as a function of temperature and CO_2 fugacity. The observed assemblage smithsonite + quartz requires high CO_2 fugacities (log f_{CO2}>0) if temperatures were higher than 40°C. Such high CO_2 fugacities would be consistent with travertine-depositing systems (e.g., Chiodini and Marini 1998; Minissale et al. 2002). At temperatures above 100–150°C, smithsonite + quartz is unlikely to be a stable paragenesis, as the necessary CO_2 fugacities would be unrealistically high (see also Brugger et al. 2003, p. 824). Figure 10b shows the stability of various Zn and As species as a function of oxygen fugacity and pH at a temperature of 50°C and a high log f_{CO2} of 2.3 $\left(a_{\sum As}= 10^{-3}, a_{\sum S}= 10^{-5}, a_{Fe}= 10^{-5}, a_{Zn}= 10^{-6}\right)$. A small field of coexisting smithsonite + arsenopyrite (±sphalerite) exists at pH values above 7.5 and very reducing conditions (log f_{O2}<−60).

Discussion

Origin of stage I carbonate ore

The Angouran deposit is located in a recently strongly uplifted, mountainous, relatively arid region, which does not have particularly favorable conditions for deep weathering of sulfides. Thus the significant and deep reaching Zn carbonate mineralization at Angouran can hardly be explained by supergene processes. The narrow, pipe-like nonsulfide ores, which contain very few relicts of primary sulfide ores but show ample evidence of marble replacement, overlie the tabular sulfide orebody like an inverted mushroom (Fig. 3), as if Zn was transported and dispersed upwards rather than

Table 7 Rb–Sr isotope data of metamorphic schists from Angouran

Sample No	Location	Composition	Rb (ppm) ±2σ	Sr (ppm) ±2σ	$^{87}Rb/^{86}Sr$ ±2σ	$^{87}Sr/^{86}Sr$ ±2σ
ANG B1	DB90-205 m	Schist with chl + qz + ms − py	12.9±0.2	30.3±0.3	1.24±0.02	0.70888±0.00001
ANG B17	DB90-2935 m	Schist with chl + qz + ms − py	30.7±0.5	11.7±0.2	7.58±0.09	0.71104±0.00002

qz quartz, chl chlorite, ms muscovite, py pyrite

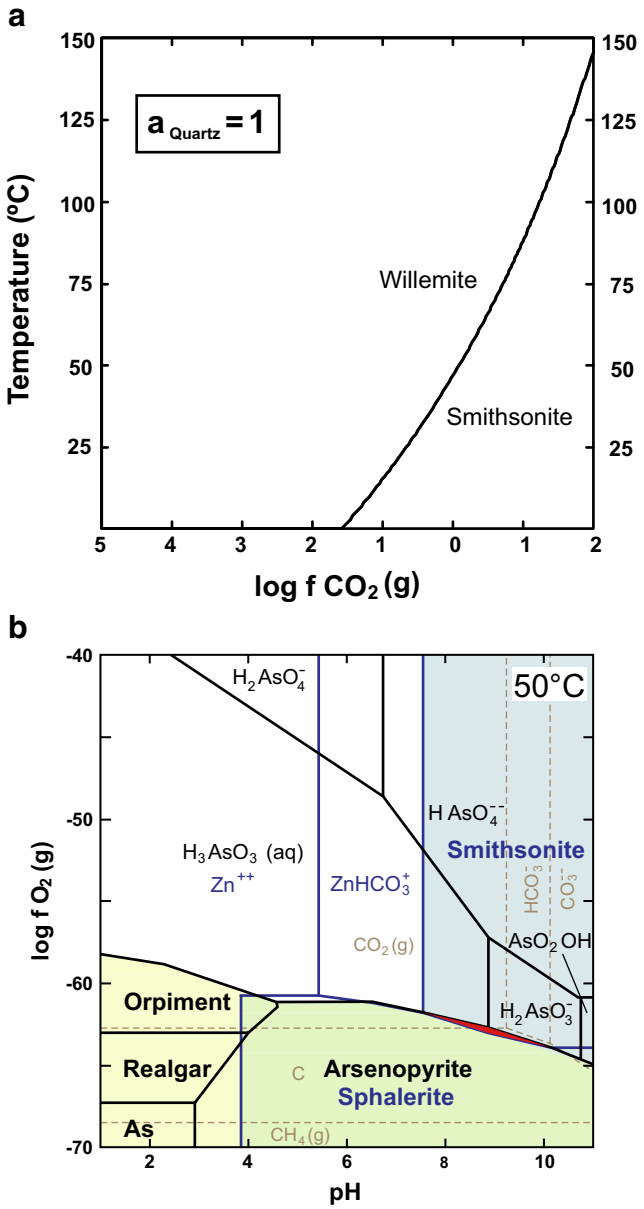

Fig. 10 **a** Stability field of smithsonite and willemite in the presence of quartz as a function of temperature and CO_2 fugacity in the gas phase. **b** Diagram to illustrate the stability fields of arsenic (*black*) and zinc (*blue*) species in the Fe–Zn–As–S–C–H–O system as a function of oxygen fugacity in the gas phase and pH at 50°C using Geochemist's Workbench and the modified Thermo2000 database (Cleverley et al. 2003). Solid phase are shown in *bold type* and their stability fields in *light colors*. The stability fields of predominant aqueous carbon species are separated by *dotted brownish lines*. Note the presence of a *small red field* of coexistence of smithsonite and arsenopyrite

laterally or downwards, as in the classical supergene wall-rock replacement model of Hitzman et al. (2003).

Furthermore, the coprecipitation of smithsonite with galena, arsenopyrite, and rare pyrite, as well as the absence of both Fe-Mn-oxides/hydroxides and typical oxidation-dissolution textures of the sphalerite-rich sulfide ore, suggest that the fluids responsible for stage I Zn carbonate ore deposition were relatively reduced (low Eh) and from slightly basic to close to neutral. On the basis of microthermometric data, fluid temperatures during precipitation were relatively low (<50°C) and salinities did not exceed those of common meteoric waters. However, the stage I Zn carbonate ore has high contents of certain elements such as Hg (25 ppm), As (14,000 ppm), Co (350 ppm), Mo (125 ppm), and Sb (440 ppm). These elements (with the exception of cobalt) are quite scarce in the primary sulfide ore (Gilg et al. 2006) but have been commonly detected in hot springs throughout the region and in the nearby Zarshuran As–Au mine. This clearly rules out the hypothesis of meteoric weathering being exclusively responsible for the formation of the nonsulfide ores at Angouran. The same elements are also contained in significant amounts in several travertine deposits of the area, such as the mine camp travertine and the Taxt-e Soleiman deposit, along with several hundreds of parts per million Zn and Pb.

The $\delta^{18}O$ values of smithsonite from the stage I carbonate ore are up to 7‰ lower and much more variable than those from carbonate-oxide ore (Fig. 8), thus indicating higher and more variable formation temperatures (consistent with the fluid inclusions data) and/or the involvement of two isotopically distinct fluid types during the stage I phase. Assuming an oxygen isotope composition of waters identical to the present-day hot springs in the area ($\delta^{18}O_{water}=-10‰$) and the new smithsonite–water fractionation equation of Gilg et al. (2007), we calculate temperatures of 40–15°C for the formation of stage I smithsonite. As exothermal sulfide oxidation can be excluded as a heat source (Gilg et al. 2007), we suggest that stage I Zn carbonate mineralization at Angouran was deposited by a distinct, low-temperature hydrothermal system, most probably related to one or more stages of Tertiary–Quaternary volcanic activity. This hypothesis is well supported by the presence of arsenopyrite in the carbonate-sulfide ore.

As shown in Fig. 10a, smithsonite (relative to willemite) is stable and coexistent with quartz in an environment with maximum temperatures of 100–120°C and very high CO_2 fugacity. High CO_2 fugacity and high pH (8–10), combined with a low oxidation state, are also required for the simultaneous deposition of arsenopyrite and smithsonite at fairly low temperatures, as deduced from the small coexistence field of both minerals resulting from the superposition of the two graphs for the As and Zn species at 50°C (Fig. 10b). These are very peculiar conditions for arsenopyrite deposition, a mineral that is generally replaced by other As minerals or by As-bearing pyrite at lower temperatures (Kretschmar and Scott 1976). We note that the paragenesis of arsenopyrite with smithsonite at Angouran is probably one of the lowest temperature occurrence (<40°C) of arsenopyrite ever recorded, as arsenian pyrite is the most common Fe-bearing arsenic phase at such low temperatures

(D.K. Nordstrom, personal communication, 2003). However, our petrographic observations and thermometric calculations and the thermodynamic models including those by Vink (1996) and Craw et al. (2003) clearly show the stability of arsenopyrite at temperatures less than 100°C. The fact that hypogene smithsonite and calcite have similar $^{87}Sr/^{86}Sr$ ratios around 0.70821–0.70895, slightly more radiogenic than those of the marbles, reflects some influence of a radiogenic source, probably the host metamorphic schists and marbles of the Angouran deposit. The Sr isotopic composition of smithsonite and calcite may reflect a mixture of Sr derived from the host marbles, with some contribution of slightly more radiogenic Sr mobilized from metamorphic schists. The Miocene two-point isochron age of 24.00±0.44 Ma given by the two analyzed schist samples, if significant, is not very far from a $^{40}Ar/^{39}Ar$ age of 20 Ma, proposed as a maximum age for the sulfide mineralization at Angouran by Gilg et al. (2006). The initial $^{87}Sr/^{86}Sr$ ratio of the two-point line is 0.70846± 0.00002, lower than the $^{87}Sr/^{86}Sr$ ratios obtained for calcite and most smithsonite samples. Therefore, the schists could have delivered slightly radiogenic Sr, to contribute to the composition of "altered" marbles and smithsonite, at any time between 24 Ma ago and the present.

Comparison of the O, C, and Sr isotope data (Fig. 9) for the host marbles of the deposit with those obtained for the clasts of the breccia ore reveals a common alteration trend expressed by a marked increase in radiogenic Sr and $\delta^{13}C$ and decrease in $\delta^{18}O$ values. This trend points towards the C, O, and Sr isotope signatures measured in calcite crystals occurring in vugs, veins, and fissures, as well as in the travertine-like formations in the Angouran marble in and around the orebody. The latter, being characterized by heavy $\delta^{13}C$ (+5) and low $\delta^{18}O$ values (+17), show a clear hydrothermal signature indicating a hydrothermal karstic environment. The fact that some calcite samples have high $\delta^{18}O$ and low $\delta^{13}C$ values implies that the main mechanism of calcite precipitation around the Angouran orebody was not simple cooling and CO_2 degassing but should have involved mixing of an ascending hot, ^{13}C-rich fluid with cold, ^{12}C-rich ground waters.

We note the high and consistent $\delta^{13}C$ values of +5‰ of the hypogene carbonate alteration, of hypogene stage 1 smithsonite, and of the Angouran mine camp travertine. This suggests a common origin of these carbonates. The carbon did not originate locally from the Angouran marble wall-rock bearing $\delta^{13}C$ values of +2‰, but from a deeper, hotter source.

Zn carbonates deposited by hypogene–hydrothermal fluids have been recorded from elsewhere in the literature, although not producing economic ore deposits. Kucha and Czajka (1984) were the first to describe "primary"-hydrothermal Zn–Pb carbonates that often precede sulfides in the carbonated-hosted Zn–Pb ores in Poland. Minčeva-Stefanova (1989) described a rare hydrothermal mineralization phase consisting of dolomite, pink cobaltian smithsonite, calcite, aragonite, and sulfides in veins and cavities of the stratiform Sedmochislenitsi Pb–Zn(–Cu) deposit, Bulgaria. Relvas et al. (2006) have recently quoted the presence of hydrothermal smithsonite (120–145°C based on oxygen isotopes) in the late alteration stages of the Neves-Corvo deposit in Portugal. One of us (CRA) has seen mylonitized, stylolitic smithsonite replacing Jurassic/Cretaceous limestone in the Orecks zinc prospect, Kayseri district, central Turkey, a district dominated by supergene smithsonite. This smithsonite-calcite assemblage has every textural indication of being a hypogene ore type along a late thrust fault. However, other Angouran-type nonsulfide deposits have not been described from elsewhere so far, not even among the "hypogene" nonsulfide ores mentioned by Hitzman et al. (2003).

Origin of stage II carbonate ore

Compared to the economic stage I carbonate ores, the stage II carbonate ores are much less voluminous. The sulfide ores at depth are shielded by the stage 1 carbonate ores from oxidation by infiltrating surface waters, and the trace amount of sulfides within stage 1 carbonate ore is not sufficient to produce a significant supergene oxidation zone. The mineralization stage that is unambiguously related to supergene weathering at Angouran is evidenced by a paragenesis mainly containing hemimorphite, smithsonite II, Fe-Mn-oxides, and Pb-Ca-arsenates occurring near the surface, where even traces of sulfides are now absent. The C–O isotope signatures (constant O isotope values and variable and light C isotope values) of smithsonite II and cerussite are quite characteristic for supergene carbonate minerals precipitated in oxidation zones (Gilg and Boni 2004a, b; Gilg et al. 2007) and distinct from stage I carbonate ores. The low but variable C isotope values of the supergene smithsonite and cerussite suggest mixing of heavy carbon derived from the wall rocks with some minor contribution of organic soil-derived or microbially derived carbon, a process also reported for supergene smithsonite deposited in Sardinia, Belgium, and Namibia (Gilg et al. 2007). We calculate temperatures of smithsonite II precipitation at about 15–20°C from their oxygen isotope data using the present-day local meteoric water isotope values and the smithsonite–water oxygen isotope fractionation equations of Gilg et al. (2007). These calculated temperatures are compatible with the average day temperatures in the area during the summer but clearly higher than the temperatures of the local cold springs.

Conclusions

The formation of the large, high-grade Angouran nonsulfide Zn deposit occurred during two successive stages.

During the first and more significant stage, the circulation of CO_2-rich hydrothermal fluids, possibly driven by the waning phases of volcanic activity in the Takab district, caused the deposition of a large amount of Zn carbonate ore (stage I carbonate ore), coexisting with and partly replacing a body of associated, primary sulfides. This could be defined as a massive carbonatization process of a sulfide orebody caused by carbonic hydrothermal fluids. We consider the age of hypogene sulfide–carbonate mineralization at Angouran (stage I carbonates) to be very young (possibly Pleistocene) due to the strict relationship between this mineralization phase and the Angouran metal-enriched travertines, which do not show any evidence of tilting or strong erosion. The very distinct main and trace element budget of the primary sulfides compared to the sulfide–carbonate ores suggests an external origin of some elements (As, Sb, and Cu) during the deposition of stage I nonsulfides. Among these, arsenic is the most important one, being abundant in stage I nonsulfides (>6,000 ppm As in the carbonate ore) in the form of arsenopyrite. Arsenic is also present in the Takab travertines (115–258 ppm As) and in several hot springs throughout the region (1.62% As in the bottom sediments of the Taxt-e Soleiman lake, Naumann 1961). This proofs a regional-scale circulation of hydrothermal fluids.

During a minor weathering phase (?Holocene), the sulfide-bearing stage I carbonate ores were partly oxidized, resulting in the deposition of small amounts of newly formed Zn carbonates, silicates, and arsenates derived from arsenopyrite oxidation (oxide-carbonate ore). The bulk of primary sulfide ores were at that time not outcropping at the surface; they were sheltered from supergene oxidation by the massive cap of hypogene Zn carbonates.

Oxygen, carbon, and strontium isotope data constrain the temperature and origin of the fluids responsible for the two Zn carbonate ore stages. The formation temperatures of stage I smithsonite were higher than the ambient temperature. The very heavy carbon isotope compositions of stage I smithsonite are similar to those of some of the hot-spring travertines in the Takab region. We interpret these heavy C isotope compositions as product of very high temperature (>500°C) decarbonatization (which might be related to contact metamorphism) and low-temperature deposition (<100°C; see Pentecost 2005). The paucity of isotopically light carbon, even in the stage II smithsonite (weathering), is indirect evidence for the absence of a significant vegetation cover at Angouran, because it is the organic matter from the soils that is usually controlling the highly variable carbon isotope distribution in supergene nonsulfide deposits (Gilg et al. 2007). Supergene stage II smithsonite formed from very light meteoric waters (−10 permil) at T<25°C, consistent with the high elevation of the deposit in relatively recent times.

The results of our study open new insights in the genesis of nonsulfide deposits because they advocate a hypogene origin for most Zn carbonate ores that are currently mined at Angouran, a presently unique process, although probably not an isolated instance. It must be kept in mind, however, that nonsulfide ores belonging to both mineralization stages in Angouran have generally lower ore grades than primary sulfide ores (Table 1), implying an overall dispersion of Zn during the carbonatization process. Nevertheless, owing to their still high metal grades (>25% Zn) and tonnages, Angouran-type nonsulfide ores would represent without doubt a most desirable exploration target, especially if cheap extraction techniques could be applied. New deposits of this type could well be encountered in other Middle East volcanic areas of recent uplift, where carbonate-hosted primary Zn-rich sulfide orebodies may have been in contact with a travertine-style hydrothermal activity.

Acknowledgements Thanks are due to M. Sadeghi (Shiraz University) for collecting part of the samples and to A.E. Annels and M. Pittuck (SRK) for providing carbonate samples from the mining district. We thank also R. Mohammadi Niaei (IZMDC) and S. Modabberi for help during fieldwork. We are indebted to F. Daliran (Karlsruhe University, Germany) and G. Borg (Halle University, Germany) for fruitful discussions. We acknowledge the help of U. Struck (LMU, Munich, Germany) and W. Stichler (GSF, Neuherberg, Germany) in measuring isotope compositions of carbonate and water samples, respectively. J. Cleverley (JCU, Townsville, Australia) kindly provided a revised version of his Thermo2000 database. This study was partly financed by funds of Università di Napoli to GB and MB.

References

Alavi M (1994) Tectonics of the Zagros orogenic belt of Iran: new data and interpretation. Tectonophysics 229:211–238

Amiri A, Rasa I (2006) Geological characteristics of the stratabound non-sulfide zinc(-lead) deposits in the Kuhbanan-Bahabad area (in farsi). Quarterly Applied Geology 2(1):1–9

Amiri A, Ghorbani M, Akbarzadeh A, Shojaei SV (2005) A new approach to the zinc and lead non-sulphide strata-bound ore deposits in the Kuhbanan-Bahabad area (in farsi). 9th Symposium of Geological Society of Iran, 30-31 August 2005, 2:375–385

Annels AE, O'Donovan G, Bowles M (2003) New ideas concerning the genesis of the Angouran Zn-Pb deposit, NW Iran. 26th Mineral Deposits Studies Group, Abstracts, University of Leicester (UK), 11–12 January 2003

Bethke CM (2002) The geochemist's workbench release 4.0: a user's guide to Rxn, Act2, Tact, react, and Gtplot. University of Illinois, Urbana, IL

Birck JL (1986) Precision K-Rb-Sr isotopic analysis: application to Rb-Sr chronology. Chem Geol 56:73–83

Boni M (2003) Non-sulfide zinc deposits: a new-(old) type of economic mineralization. SGA News Nr. 15 (August 2003), 1 and 6–11

Borg G (2005) Geological and economical significance of supergene nonsulphide zinc deposits in Iran and their exploration potential. In: Geological Survey of Iran (ed): Mining and Sustainable Development. 20th World Mining Congress, Tehran, Iran, 7–11 November 2005, pp 385-390

Borg G, Daliran F (2004) Hypogene and supergene formation of sulphides and non-sulphides at the Angouran high-grade zinc deposit, NW-Iran. In: Abstract volume of geoscience Africa 2004. University of the Witwatersrand, Johannesburg, pp 69–70

Brugger J, McPhail DC, Wallace M, Waters J (2003) Formation of willemite in hydrothermal environments. Econ Geol 98:819–835

Chiodini G, Marini L (1998) Hydrothermal gas equilibria; the H_2O-H_2-CO_2-CO-CH_4 system. Geochim Cosmochim Acta 62:2673–2687

Cleverley JS, Benning LG, Mountain BW (2003) Reaction path modeling in the As-S system: a case study for geothermal As transport. Appl Geochem 18:1325–1345

Craw D, Falconer D, Youngson JH (2003) Environmental arsenopyrite stability and dissolution: theory, experiment, and field observations. Chem Geol 199:71–82

Daliran F, Borg G (2003) A preliminary appraisal of the non-sulphide zinc deposit of Angouran, North-West Iran. In: Eliopoulos D et al. (eds) Mineral exploration and sustainable development, Millpress, Rotterdam, pp 65–68

Daliran F, Borg G (2005a) Characterisation of the nonsulfide zinc ore at Angouran, northwestern Iran, and its genetic aspects. In: Jingwen M, Bierlein FP (eds) Mineral deposit research: meeting the global challenge, vol 2. Springer, Berlin Heidelberg New York, pp 913–916

Daliran F, Borg G (2005b) Genetic aspects of the Angouran non-sulphide zinc ore deposit, NW-Iran, as an exploration guide for nonsulphide zinc ores. "Mining and Sustainable Development," 20th World Mining Congress & Expo 2005, Tehran, Iran, 7–11 November 2005, 6 pp

Damm B (1968) Geologie des Zendan-i Suleiman und seiner Umgebung südöstliches Balqash-Gebirge Nordwest-Iran. Beiträge zur Archäologie und Geologie des Zendan-i Suleiman, Teil 1, Franz Steiner Verlag, Wiesbaden. 1–52

Farpoor MH, Khademi H, Eghbal MK, Krouse HR (2004) Mode of gypsum deposition in southeastern Iranian soils as revealed by isotopic composition of crystallization water. Geoderma 121 (3–4):233–242

Gat JR, Carmi I (1970) Evolution of the isotopic composition of atmospheric waters in the Mediterranean Sea area. J Geophys Res 75:3039–3048

Gat JR, Dansgaard W (1972) Stable isotope survey of the fresh water occurrences in Israel and the Northern Jordan. J Hydrol 16:177–212

Gazanfari F (1991) Metamorphic and igneous petrogenesis in NE of Takab with special regard to zinc mineralization in the Angouran mine. Master's thesis, University of Teheran, Iran (in Farsi)

Geological Survey of Iran (1999) Geological map of Iran, 1: 100,000 Series Sheet Takht-e-Soleiman

Ghazban F, McNutt RH, Schwarcz HP (1994) Genesis of sediment-hosted Zn-Pb-Ba deposits in the Irankuh district, Esfahan area, West-Central Iran. Econ Geol 89:1262–1278

Gilg HA, Boni M (2004a) Role of stable isotope studies on Zn and Pb carbonates in mineral exploration of large non-sulphide deposits. 32nd Int Geol Congr, 2004, Abs.Vol., pt. 2 abs 245–12, p. 1105

Gilg HA, Boni M (2004b) Stable isotope studies on Zn and Pb carbonates: Could they play a role in mineral exploration? Proceedings of ICAM 2004, 4 p

Gilg HA, Allen C, Balassone G, Boni M, Moore F (2003a) The 3-stage evolution of the Angouran Zn "oxide"-sulphide deposit, Iran. In: Eliopoulos D et al. (eds) Mineral exploration and sustainable development. Millpress, Rotterdam, pp 77–80

Gilg HA, Struck U, Vennemann T, Boni M (2003b) Phosphoric acid fractionation factors for smithsonite and cerussite between 25 and 72°C. Geochim Cosmochim Acta 67:4049–4055

Gilg HA, Boni M, Balassone G, Allen CR, Banks D, Moore F (2006) Marble-hosted sulfide ores in the Angouran Zn-(Pb-Ag) deposit, NW Iran: interaction of sedimentary brines with a metamorphic core complex. Miner Depos 31(1):1–16

Gilg HA, Boni M, Hochleitner R, Struck U (2007) Stable isotope geochemistry of carbonate minerals in nonsulfide Zn-Pb deposits. Ore Geol. Rev. (in press)

Glennie KW (2000) Cretaceous tectonic evolution of Arabia's eastern plate margin: a tale of two oceans. In: Middle East models of Jurassic/Cretaceous carbonate systems. SEPM Special Publication No. 69, pp 9–20

Götte T, Richter DK (2004) Quantitative high-resolution cathodoluminescence spectroscopy of smithsonite. Mineral Mag 68:199–207

Hamdi B (1995) Precambrian-Cambrian deposits in Iran. In: Hushmandzadeh A (ed) Treatise of the geology of Iran, vol 20. Geological Survey of Iran, Tehran, pp 1–535

Hitzman MW, Reynolds NA, Sangster DF, Allen CR, Carman CE (2003) Classification, genesis, and exploration guides for nonsulfide zinc deposits. Econ Geol 98:685–714

Horwitz EP, Dietz ML, Fischer DE (1991a) SREX: a new process for the extraction and recovery of strontium from acidic nuclear waste streams. Solv Extr Ion Exch 9:1–25

Horwitz EP, Dietz ML, Fischer DE (1991b) Separation and preconcentration of Sr from biological, environmental and nuclear waste samples by extraction chromatography using a crown ether. Anal Chem 63:522–525

Houtum-Schindler A (1881) Neue Angaben über die Mineralreichthümer Persiens und über die Gegend westlich von Zendjan. Jb kaiserl kgl Geol Reichsanst 31:169–190

Kretschmar U, Scott SD (1976) Phase relations involving arsenopyrite in the system Fe-As-S and their application. Can Mineral 14:364–386

Kucha H, Czajka K (1984) Sulphide-carbonate relationships in the Upper Silesian Zn-Pb deposits (Mississippi Valley-type), Poland, and their genesis. Trans Inst Min Metall 93:12–22

Large D (2001) The geology of non-sulphide zinc deposits—an overview. Erzmetall 54:264–276

Lohmann KC (1988) Geochemical patterns of meteoric diagenetic systems and their application to studies in paleokarst. In: James PN, Choquette PW (eds) Paleokarst. Springer, Berlin Heidelberg New York, pp 58–80

Ludwig KR (2003) Users manual for ISOPLOT/Ex rev. 2.49. A geochronological toolkit for Microsoft Excel. Berkeley Geochron Cent Spec Pub 1a: pp. 56

Minčeva-Stefanova J (1989) New facts concerning the formation of hydrothermal sphalerite-smithsonite parageneses. Dokl Bolg Akad Nauk 42:93–96

Minissale A, Kerrick DM, Magro G, Murrell MT, Paladini M, Rihs S, Sturchio NC, Tassi F, Vaselli O (2002) Geochemistry of Quaternary travertines in the region north of Rome (Italy): structural, hydrologic and paleoclimatic implications. Earth Planet Sci Lett 203:709–728

Moradi S, Koleini SMJ, Hedjazi F (2004) Thermal treatment of Angouran lead and zinc flotation plant oxidised tailings, Iran. Green Processing 2004, 10–12 May 2004 Fremantle WA. Conference Proceedings AusIMM: 233–236

Moser H, Stichler W (1980) Isotopenhydrologische Untersuchungen im Karstgebiet zwischen Dasht-e Arjan und Kazerun (Zagros-Gebirge, Iran). GSF-Bericht R250, 39–50

Naumann E (1961) Geographische und geologische Einordnung. Teheran Forsch 1:15–32

Pentecost A (2005) Travertine. Springer, Berlin Heidelberg New York

Pokrovski GS, Kara S, Roux J (2002) Stability of arsenopyrite, FeAsS, in crustal fluids. Geochim Cosmochim Acta 66:2361–2378

Pouchou JL, Pichoir F (1991) Quantitative analysis of homogeneous or stratified micro-volumes applying the model "PAP". In: Heinrich KFJ, Newbury DE (eds) Electron Probe Quantification. Plenum, New York, pp 31–75

Relvas JMRS, Barriga FJAS, Longstaffe FJ (2006) Hydrothermal alteration and mineralization in the Neves-Corvo volcanic-hosted massive sulfide deposit, Portugal. II. Oxygen, hydrogen and carbon isotopes. Econ Geol 101:791–804

Roedder E (1984) Fluid Inclusions. Rev Miner 12:1–646

Salomons W, Mook WG (1986) Isotope geochemistry of carbonates in the weathering zone. In: Fritz P, Fontes JC (eds) Handbook of Environmental Isotope Geochemistry, vol. 2. Elsevier, Amsterdam, The Netherlands, pp 239–269

Savelli C, Wedepohl KH (1969) Geochemische Untersuchungen an Sinterkalken (Travertinen). Contrib Mineral Petrol 21:238–256

Stockli DF, Hassanzadeh J, Stockli LD, Axen G, Walker JD, Dewane TJ (2004) Structural and geochronological evidence for Oligo-Miocene intra-arc low-angle detachment faulting in the Takab-Zanjan area, NW Iran. Abstr Programs Geol Soc Am 36(5):319

Talma AS, Netterberg F (1983) Stable isotope abundances in calcretes. In: Wilson RCL (ed) Residual deposits: surface related weathering processes and materials. Geol Soc London Spec Pub 11, Blackwell, Oxford, pp 221–233

Turi B (1986) Stable isotope geochemistry of travertines. In: Fritz P, Fontes JC (eds) Handbook of Environmental Isotope Geochemistry, vol. 2. Elsevier, Amsterdam, The Netherlands, pp 207–238

Vink BW (1996) Stability relations of antimony and arsenic compounds in the light of revised and extended Eh-pH diagrams. Chem Geol 130:21–30